ABSTRACT

Title of Thesis: SEMI-ADAPTIVE INFUSION CONTROL OF MEDICATIONS WITH EXCITATORY DOSE-DEPENDENT EFFECTS

Junxi Zhu, Master of Science, 2017

Thesis directed by: Assistant Professor Jin-Oh Hahn
Department of Mechanical Engineering

This thesis presents a semi-adaptive closed-loop control approach to infusion of medications that exhibit excitatory dose-dependent effects. A unique challenge associated with closed-loop control of such medications is that the upper bound of medication-induced excitatory response is unknown and cannot be readily incorporated into control design. To address this challenge, we developed a new dose-response model by extending a classical dose-response model, used for medications with depressive effects, by a nonlinear transformation, and extended a semi-adaptive control approach developed in our prior work, applicable to depressive dose-response relationship, to the new dose-response model. Two key advantages of the proposed model are that it can capture dose-response relationship from baseline to a target set point, and that it enables linear parameterization, thereby facilitating the control design task. We examined the efficacy of the proposed approach using an example of heart rate response to a vasoactive medication norepinephrine. System identification analysis using experimental data and in-silico controller testing showed that

the new dose-response model could faithfully reproduce the experimental data, and that the semi-adaptive controller could effectively regulate the response in a wide range of simulated subjects.

SEMI-ADAPTIVE INFUSION CONTROL OF MEDICATIONS WITH EXCITATORY DOSE-DEPENDENT EFFECTS

by

Junxi Zhu

Thesis submitted to the Faculty of the Graduate School of the
University of Maryland, College Park in partial fulfillment
of the requirements for the degree of
Master of Science
2017

Advisory Committee:
Assistant Professor Jin-Oh Hahn, Chair/Advisor
Professor Miao Yu
Professor Nikhil Chopra

Acknowledgments

I owe my gratitude to all the people who have made this thesis possible and because of whom my graduate experience has been one that I will cherish forever.

First and foremost I'd like to thank my advisor, Dr. Hahn for giving me an invaluable opportunity to work in his lab. His continuous support and guidance is the foundation on which I would be able to finish this work. Also, I am extremely grateful that he has always been patient when I repeatedly made stupid mistakes. It has been a pleasure to work with and learn from such an extraordinary individual. I hope that my work can help Dr. Hahn and the rest of the lab move further on the current projects.

I would also like to thank my colleagues at the lab, especially Ramin Bighamian and Xin Jin. They have been answering my endless questions and helping me to understand concepts that I was not familiar with. My work would not have been possible without their extraordinary ideas.

My housemates at my place of residence have been a crucial factor in my finishing smoothly. I'd like to express my gratitude to Xin Jin, Haoyuan Jing, Liang He, Tu Shi for their friendship and support and especially to Zehua Zeng, who has prepared and cooked numerous dishes for me.

My sincere thanks and gratitude go to Professor Nikhil Chopra and Professor Miao Yu for agreeing to be on my thesis committee. I truly appreciate your time and effort on evaluating this manuscript.

I would also like to acknowledge help and support from the Office of Naval

Research (ONR) under Grant No. N000141410591 and N000141512018. This work would not have been possible without their funding.

I owe my deepest thanks to my family - my mother and father who have always stood by me and guided me through my career, and provided financial support that enables me to study at the U.S.. Words cannot express the gratitude I owe them.

Table of Contents

List of Tables

List of Figures

List of Abbreviations

BIS	Biospectral index
DDDR	Direct dynamic dose-response
DoH	Degree of hypnosis
HR	Heart rate
IV	Intravenous
MAP	Mean arterial pressure
NE	Norepinephrine
PD	Pharmacodynamics
PK	Pharmacokinetics
RR	Respiratory rate
SBP	Systolic blood pressure
SVR	Systemic vascular resistance
TCI	Target-controlled infusion
WAV_{CNS}	Wavelet-based index

Chapter 1: Introduction

1.1 Use of Vasopressor

Shock, which normally means a lack of blood flow to a specific area of the body, results in the oxygen and nutrients not being able to be delivered to the tissues and thus is a life-threatening situation. Shock comes in a variety of forms: septic shock, which occurs as a consequence of the inflammatory response to infection, can lead to respiratory or heart failure. Cardiogenic shock, which in contrast is mostly often triggered by a heart attack, causes a decrease in the cardiac output and thus leads to hypoperfusion and hypotension. Hypotension is usually defined by a drop in systolic blood pressure (SBP) to < 90 mmHg or by at least a 40-mmHg decrease from baseline. The inadequate perfusion to critical organs (heart, liver and kidneys) will lead to significant mortality reported to be around 40% to 60% [1]. Septic shock is also reported to be account for 18% to 50% of ICU mortality [2]. Once septic shock is formed, immediate and aggressive medical attention is needed. Early effective fluid resuscitation is crucial to stabilize the resulting tissue hypoperfusion. To achieve adequate fluid resuscitation, the Surviving Sepsis Guidelines advise at least 30 ml/kg of crystalloids be infused for most patients in septic shock and fluid should be aggressively infused for as long as the patient continues to improve hemodynamically

[2]. Despite fluid resuscitation, vasopressors should be promptly begun in patients in persistent septic shock. There are a variety of available vasopressors for the clinicians to use (see Table. 1.1), however, making recommendations on the use of a specific vasopressor is made difficult by the limited number of controlled experiments and the fact that these agents are usually used in combination [3]. No study to date has demonstrated a significant benefit on survival rate of one vasopressor on another [4], therefore the choice of vasopressor is pretty much empiric. Yet the Surviving Sepsis Campaign recommends norepinephrine (NE) or dopamine as the first-line agent on patients presenting septic shock followed by epinephrine to those who respond poorly to norepinephrine or dopamine [5].

Table 1.1: Vasopressor drug name, clinical indication for therapeutic use, standard dose range and receptor binding [6].

			Receptor Binding		
Drug	Clinical Indication	Dose Range (IV)	α_1	β_1	β_2
Dopamine	Shock (cardiogenic, vasodilatory)	2.0-20 mcg/kg/min	+++	++++	++
Dobutamine	Low CO (myocardial dysfunction)	2.0-20 mcg/kg/min	+	+++++	+++
Norepinephrine	Shock (vasodilatory, cardiogenic)	0.01-3.0 mcg/kg/min	+++++	+++	++
Epinephrine	Shock (vasodilatory, cardiogenic)	0.01-0.1 mcg/kg/min	+++++	++++	+++
Isoproterenol	Bradyarrhythmias	2-10 mcg/kg/min	0	+++++	+++++
Phenylephrine	Hypotension	0.4-9.1 mcg/kg/min	+++++	0	0

α_1 indicates α-1 receptor; β_1, β-1 receptor; β_2, β-2 receptor; 0, zero significant receptor affinity; + through +++++, minimal to maximal relative receptor affinity; mcg refers to μg.

1.2 Vasopressor Dose-Response Modeling

Vasopressors take effect on the cardiovascular endpoints (e.g. heart rate, cardiac output, mean arterial pressure, systemic vascular resistance) through stimulus of different receptors. Activation of α_1-adrenergic receptors on arterial vascular smooth muscle cells results in smooth muscle contraction and an increase in systemic vascular resistance (SVR), while β_1-adrenergic receptor stimulation results in enhanced myocardial contractility and stimulation on β_2-adrenergic receptor results in vasodilation [6]. The actual underlying mechanism of vasopressors is by all means much more complicated than this and thus make it extremely difficult to accurately describe and model this entire process. However, in the real hospital settings, clinicians rarely dig this deep into the exact mechanism of a specific drug. Instead, they tend to use a simplified model to help them determine how much drug should be infused to a patient's body. For example, they may determine using their experience that a certain dose level of the drug is needed to alter the endpoints to achieve a desired set point. Such a simplified model is called a drug effect model, which describes the relationship between the infusion dose and the change in the endpoints. The drug effect model is typically consisted of two parts, the pharmacokinetics (PK) part and the pharmacodynamics (PD) part. The pharmacokinetics (PK) part of the model describes how the infused drug is distributed in the patient's body while the pharmacodynamics (PD) part relates the effect site dose to the endpoints.

The most popular PK model is the compartmental model [7,8], which can further be divided into smaller categories depending on how many compartments are

used in the model. The compartmental model divide the human body into several portions (e.g., tissues, organs, blood) and assign different rates to each compartment to model the absorption and eliminations of drugs. The drug concentration is assumed to be homogeneous in each compartment and the transmission of drug between one compartment to another is purely driven by the difference in the concentration. The output of the PK model is the plasma concentration C_p. The PD model in general consists of a first order system (which transforms the plasma concentration C_p to effect site concentration C_e) and a model that describes the concentration-effect relationship. This model is usually chosen to be the Emax model, which utilizes a empirical nonlinear Hill curve to relate the effect site concentration by either IV infusion or oral absorption to the corresponding change in the endpoint.

1.3 Closed-Loop Control

In a surgery, it is usually desirable (sometimes necessary) for the clinicians to control a set of physiologic indexes (e.g., heart rate, mean arterial pressure, cardiac output) and hold them within a specific range. Take anesthesia as an example, closed-loop control of medication infusion has been an active field of research for a few decades in critical care medicine, with a large number of work reported on closed-loop control of anesthesia, analgesia, and neuromuscular blockade [9–12]. Traditionally, the clinicians manually control the drug administration which is based on their experience, established rules and the measured/predicted patient response.

In this process, the expert opinion and knowledge is very important because human body is a sophisticated system and thus suffers from a large intervariability and intravariability. Besides, manual administration is also prone to human error and the heavy work load restricts the ability of clinicians to perform other high-level tasks.

A computer program, on the other hand, can be used to assist the drug administration using the prior computation of the dose profile. This is implemented by a Target-Controlled Infusion (TCI) system [13, 14]. However, TCI is only a open-loop system rather than a closed-loop system. Since TCI uses pharmacokinetics/pharmacodynamics (PKPD) models to predict the patient response and in real clinical settings real-time plasma/blood drug concentration is extremely difficult, if not impossible, to obtain. TCI actually estimates the drug concentration rather than obtains it through measurement, and thus the performance hinges heavily on the accurateness of the patient model. Yet, a variety of factors can alter the patient's physiological condition, e.g., surgical stimulation and hypnotic-opioid synergy. Thus, in the end, TCI still requires human interventions to function properly.

Hence, a more advanced automatic infusion system should have the ability to adapt itself to different patient conditions. This can be achieved by introducing a closed-loop control scheme to the system. The advantages of using closed-loop infusion system over manual administration have been confirmed by many literatures [15–17], which include smaller steady-state error, improved hemodynamic stability, shorter recovery time and optimized drug use. To achieve accurate feedback, the process itself should be defined and representative measures of the system state

should also be available. Again using controlled anesthesia as an example, clinicians typically choose compartmental models to describe the drug distribution and indexes like BIS [18] or WAV_{CNS} [19] as a measure of degree of hypnosis (DoH). These endpoints have definitive bounds with upper bound being the nominal value and zero being the lowest possible value. The boundedness of the range of response with its explicit limits facilitated the use of classical dose-response models, e.g., the Emax model [20], in designing closed-loop controllers for infusion of these medications (see, e.g., [18, 21–28]).

In contrast to the above, medications such as vasopressors and inotropes exhibit excitatory dose-dependent effects. A unique challenge associated with closed-loop control of such medications is that the upper limit of medication-induced excitatory response (a parameter that must be specified to characterize the Emax model) is unknown. In fact, it is extremely difficult, if not impossible, to determine the upper limit of response in a patient in real clinical settings due to patient safety and ethical considerations. Despite this prominent challenge, there has not been rigorous research effort to establish model-based closed-loop control techniques for infusion of these medications.

1.4 Thesis Goal and Outline

In an attempt to address this challenge, we present in this thesis a semi-adaptive closed-loop control approach to infusion of medications that exhibit excitatory dose-dependent effects. We will present a new dose-response model by

extending a classical dose-response model, used for medications with depressive effects, by a nonlinear transformation, and extend a semi-adaptive control approach developed based on a prior work, applicable to depressive dose-response relationship, to the new dose-response model. Two key advantages of the proposed model are that it can capture dose-response relationship from baseline to a target set point, and that it enables linear parameterization, thereby facilitating the control design task. We will examine the efficacy of the proposed approach using an example of heart rate (HR) response to a vasoactive medication norepinephrine (NE).

The thesis is organized as follows. In Chapter 2, we will present several potential candidates to replace the traditional Emax model and discuss a little about their respective structures. In Chapter 3, we will apply these candidate models to a dataset from an animal experiment, perform system identification and sensitivity analysis and eventually pick out the best candidate model. In Chapter 4, we will apply a previously developed semi-adaptive control scheme to the new model and evaluate its performance through in-silico simulation. The thesis concludes with Chapter 5 summarizing conclusions and outlining future work.

Chapter 2: Excitatory Dose-Response Modeling

2.1 Overview

In this chapter, we will first briefly introduce existing models that describe the drug distribution process and dose-response relationship. Then we will point out the issue with the existing models and present how we develop the new models based on them. After that, we will briefly compare the new models with existing ones and identify their pros and cons.

2.2 Existing Models

2.2.1 Pharmacokinetics/Pharmacodynamics Models

To investigate the effect of NE on different endpoints (heart rate, mean arterial pressure, total peripheral resistance, etc.), a pharmaceutical model is needed to describe the process of the drug being absorbed by the patient and producing desired effects at the effect site. Traditionally, a pharmacokinetics/pharmacodynamics (PKPD) model is used to describe such process. The pharmacokinetics (PK) part of the model provides the concentration-time profile in the patient body fluid (normally plasma or whole blood) with respect to the administered dose via intravenous

(IV) infusion or oral absorption. Compartmental pharmacokinetics models are widely used for this purpose [7]. The most simple compartmental model is the one-compartment model depicted in Fig. 2.1.

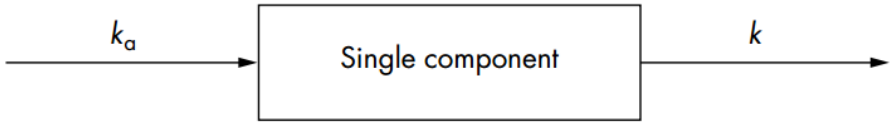

Figure 2.1: One-Compartment model. k_a=absorption rate constant, k=elimination rate constant. [29]

In this model, the drug is assumed to achieve instantaneous distribution throughout the body and that the drug equilibrates instantaneously between tissues [29]. More complex multi-compartmental models have also been developed to account for sophisticated dynamics for some drugs. A two-compartmental model, which resolves the body into a central compartment and a peripheral compartment as shown in Fig. 2.2.

In the two-compartment model, it is assumed that the drug distributes between central and peripheral compartment and that the drug does not achieve instantaneous equilibrium between two compartments [29]. A three-compartment model, which further divides the peripheral compartment into fast-response and slow-response compartments is also available and frequently used.

On the other hand, the pharmacodynamics (PD) model first transforms the plasma concentration C_p from the PK model to effect site concentration C_e through a first-order transfer function and then relates C_e to the observed endpoint effects.

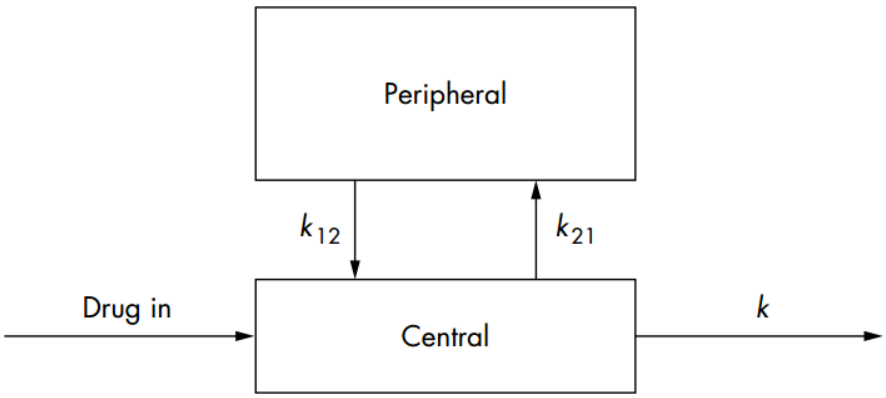

Figure 2.2: Two-Compartment model. k_{12}, k_{21} and k are first-order rate constants: k_{12}=rate of transfer from central to peripheral compartment; k_{21}=rate of transfer from peripheral to central compartment; k=rate of elimination from central compartment [29].

There exists various kinds of PD model, among which are (sigmoid) E_{max} model, (sigmoid) I_{max} model, logarithmic model quadratic model, etc. The most frequently used PD model is the sigmoid E_{max} model, which utilizes nonlinear Hill equation to describe nonlinear concentration-effect relationships [7]. It has the general form:

$$E = E_0 + \frac{E_{max} C^{\lambda}}{EC_{50}^{\lambda} + C^{\lambda}} \tag{2.1}$$

where the effect E is a function of E_0, the baseline value of the endpoint, E_{max}, the maximum effect, C, the concentration of the drug, EC_{50}, the concentration of drug that produces half of the maximal effect and λ, the Hill coefficient, which determines the shape of the nonlinear curve.

2.2.2 Direct Dynamic Dose-Response Models

Despite of the traditional PKPD model, a direct dynamic dose-response (DDDR) model is proposed by Hahn et al. [30], whose structure is shown in Fig. 2.3. Compared with PKPD model, the DDDR model directly links the infusion dose to the endpoint effect, i.e., the true infusion rate I_p is first transformed into hypothetical dose at the site of action (I_e) and then it is related to the desired endpoints via Emax model.

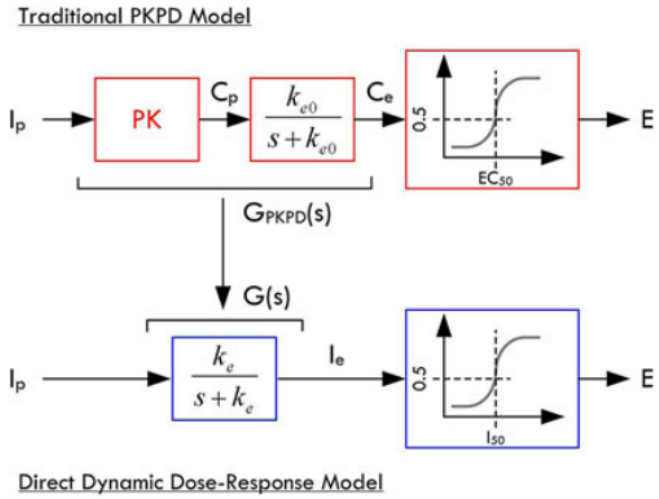

Figure 2.3: Traditional PKPD versus direct dynamic dose-response model. [30]

Note that the Emax model used in the PKPD model and in the DDDR model exhibit a slight difference, i.e., the Emax model in the PKPD model relates the effect site concentration to the clinical effect, whereas the Emax model in the DDDR model relates the effect site dose rate to the clinical effect. Therefore, EC_{50} in the PKPD model, which represents the concentration of drug at the effect site that produces 50% clinical effect is replaced by I_{50}, which represents the effect site dose rate that

produces 50% clinical effect. Also note that the transfer function $G(s)$ in the DDDR model has an unity gain, allowing effect site dose I_e to reach infusion dose I_p in the steady state.

$$E = BL + E_{max} \frac{I_e^\lambda}{I_e^\lambda + I_{50}^\lambda} \tag{2.2}$$

2.2.3 The New Model

The new model proposed by us in this thesis originates from a prior work by Jin et al. [31], where closed-loop control of anesthesia via propofol infusion is the subject of study. DDDR model along with the Emax model were utilized in that work to regulate the respiratory rate (RR) and satisfactory performance was achieved in the simulation. The endpoint (RR) in that work has definitive bounds, with its nominal value as an upper bound and zero (0) as a physical lower bound. However, there is no clear physical upper bound as of heart rate, nor it is easy to determine a physiological upper bound above which the patient may die from heart failure due to patient safety concerns and ethical reasons. To migrate the success in the propofol case to that in the norepinephrine case, we resolve this issue by assuming that the upper limit is unbounded (i.e., ∞, and this assumption will be justified later in Chapter 3.4). Specifically speaking, we want to find a map that transforms the upward-going endpoint response w.r.t effect site dose (I_e) to the downward-going endpoint response as in the propofol case. Then this is equivalent to finding a function that transforms the delta change of endpoints (ΔHR in this case) ranging from a finite number to infinity to within a finite range (i.e., from zero

to the baseline value) as shown in Fig. 2.4. One possible family of functions is the so called logistic functions which have a domain ranging from $-\infty$ to ∞ but can only take a finite range of values.

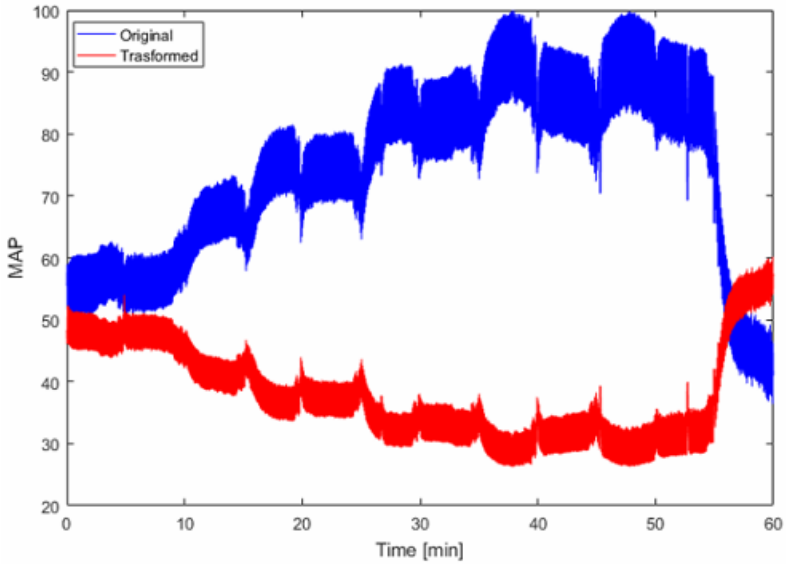

Figure 2.4: Original norepinephrine response and transformed response.

The two logistic functions considered in this report are inverse tangent function and the modified exponential function

$$BL \times \tan^{-1}\left(\frac{\Delta HR}{BL}\right) \times \frac{2}{\pi} = -\Delta HR = BL \times \frac{I_e^\lambda}{I_e^\lambda + I_{50}^\lambda} \quad \text{(Atan model)} \tag{2.3}$$

$$BL\left(\frac{2}{1+\exp(-\Delta HR/BL)} - 1\right) = -\Delta HR = BL \times \frac{I_e^\lambda}{I_e^\lambda + I_{50}^\lambda} \quad \text{(Exp model)} \tag{2.4}$$

Rewriting the above models we have

$$E = BL + BL \times \tan\left(\frac{\pi}{2}\frac{I_e^\lambda}{I_e^\lambda + I_{50}^\lambda}\right) \quad \text{(Atan model)} \tag{2.5}$$

$$E = BL - BL \times \ln\left(\frac{I_{50}^\lambda}{2I_e^\lambda + I_{50}^\lambda}\right) \quad \text{(Exp model)} \tag{2.6}$$

Here the delta change (ΔHR in this case) is normalized by its baseline value so that its magnitude is consistent when applying the map to different endpoints.

However, it should be noted that I_{50} in these two models does not have the same meaning as in the first two models. In fact, it is no longer the dose level at which half of the maximum effect is achieved. To compensate for this, we need to multiply a constant coefficient to the equation. We further see that by multiplying another coefficient σ to the equation, these models can be adapted to describe endpoint behavior of different increase amplitudes. Now the equations become

$$E = BL + BL \times \sigma\% \times \tan\left(\frac{\pi}{2}\frac{I_e^\lambda}{I_e^\lambda + I_\sigma^\lambda}\right) \quad \text{(Atan model)} \tag{2.7}$$

$$E = BL + \frac{BL \times \sigma\%}{\ln(1/3)} \times \ln\left(\frac{I_\sigma^\lambda}{2I_e^\lambda + I_\sigma^\lambda}\right) \quad \text{(Exp model)} \tag{2.8}$$

The variable I_{50} in the first two models have become I_σ in these two models which, depending on the value of σ, represents the dose level at which $\sigma\%$ of the maximum effect is achieved. The significance of σ will be discussed briefly in Chapter 2.3 and in detail in Chapter 3.4.

2.3 Model Comparison and Discussion

It should be noted that although traditional PKPD model in theory offers more accurate description of drug kinematics/dynamics than the DDDR model, it requires plasma/blood NE concentration to train the PK model. Since real-time drug concentration is usually not easily obtained, if not impossible, a population PKPD model for a specific group is used which suffers from large inter-individual as well as intra-individual variability [32]. If one insists to fit the endpoint data without plasma/blood NE concentration, it has to be estimated by the population-based PK model and then passed to the PD model. But then we might well have

omitted this step and used DDDR model in the first place. That being said, we are not to criticize the goodness of the PKPD model compared with the DDDR model, but the fact that the lack of real-time plasma/blood NE concentration in the experiment data makes the choice of adopting DDDR model instead of PKPD model inevitable.

Now that the model that relates infusion dose to effect site dose has been chosen, here comes the time to determine how to connect the effect site dose to the endpoint response. Among all three nonlinear models we have introduced in the previous section, Emax model is inarguably the most popular and widely-used dose-response model [33]. The Emax model [20] utilizes a nonlinear Hill curve to model the dose-response relationship. The parameter λ is in general larger than 1, resulting in a $\Delta E - dose$ curve with a slight increase at the beginning, a rapidly ascending stage in the region near I_{50} and a convergent phase at the end as shown in Fig. 2.5. In the traditional Emax model, the maximum increase of the endpoint is specified by the parameter E_{max}, which is normally taken to be the maximum theoretically allowed increase. Hence, this number is usually far greater than the actual increase in the experiments, which will cause problem when performing system identification. This is due to the fact that the actual dose given to the test subject is usually small compared with I_{50} value, and hence the identified I_{50} will be out of the range of the dose given, making it hard to verify its accurateness. One possible way to remedy this is to redefine E_{max} to be the maximum endpoint change that is actually achieved (instead of maximum therapeutically allowed increase) w.r.t the dose profile. However, this requires that E_{max} be related to specific dose profile

which is even hard to achieve and nearly impossible if it is to be implemented by a controller. To resolve this issue, we assume that the upper limit of the endpoint is unbounded (i.e., ∞). In fact, it is a reasonable simplifying assumption as long as medication is infused at therapeutic low-dose rates.

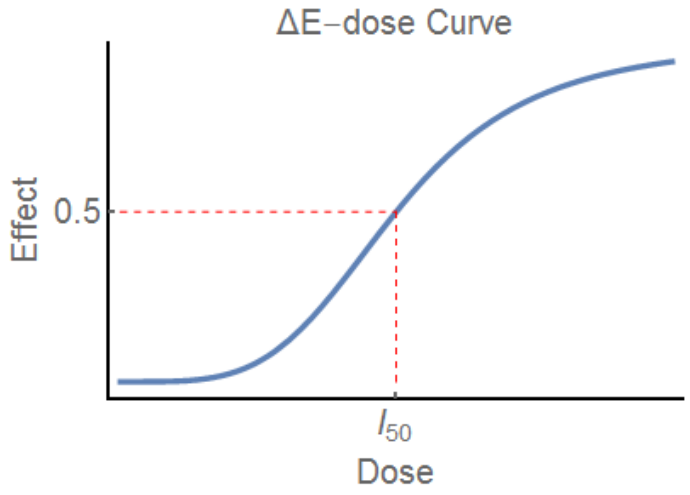

Figure 2.5: The $\Delta E - dose$ curve for the Emax model.

The remaining two models, i.e., the Atan model and the Exponential model, inherit the spirit of the traditional Emax model but with some extra modifications so that they allow the endpoint to become infinity while the dose goes to infinity. In real clinical settings, however, the dose is never going to be near infinity. Indeed, it will rarely exceed the suggested dose level of that specific drug by too much, and thus we do not need to worry about the behavior at the extremely-high dose region of these models. Yet for the Atan model, we can observe from its $\Delta E - dose$ curve from Fig. 2.6 that for typical increase magnitude (20%-100% of the baseline) of the heart rate, it does not exhibit a three-phase behavior as the Emax model either. Indeed, ΔE for Atan model increases more and more quickly when the dose exceeds

I_{50} (since the derivative of the tangent function goes to infinity at $\pi/2$), it is also not an ideal candidate to replace the Emax model either. To be more precise, the Atan model can only mimic the $\Delta E - dose$ behavior of the Emax model up to a certain point (around I_{50}) after which the $\Delta E - dose$ curve for the Emax model becomes concave while that of the Atan model remains convex.

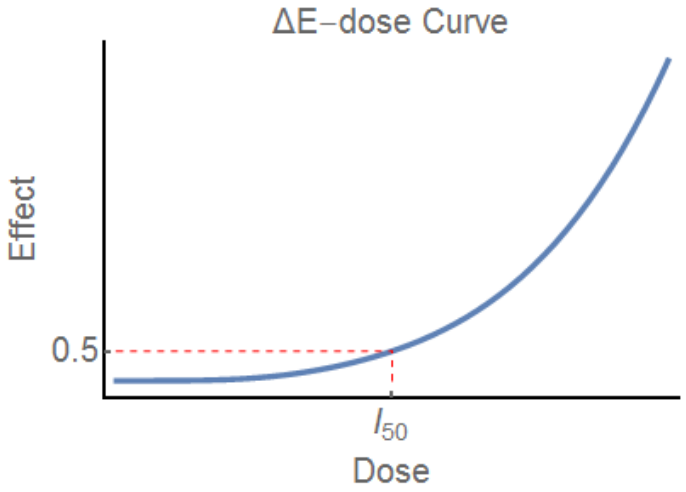

Figure 2.6: The $\Delta E - dose$ curve for the Atan model.

For the Exponential model, since the derivative of the natural log function approaches zero at the infinity, the $\Delta E - dose$ curve as shown in Fig. 2.7 gets flatter and flatter when dose increases. It can also be observed from the $\Delta E - dose$ curve that Exponential model clearly exhibits a three-phase behavior as the Emax model. And since by model design the endpoint would go to infinity when dose is infinitely large instead of converging to a specific value as the Emax model, and that is where the parameter σ kicks in. By introducing the parameter σ, the model output is set to reach $\sigma\%$ of the increase from the baseline when effect site dose I_e reaches corresponding I_σ. In a target-control-infusion (TCI) system, the desired

endpoint level that is to be reached is always known before hand, and thus σ could be set properly using this information. Besides by doing so, the I_σ identified by the controller is guaranteed to be the same as the dose level required to raise the endpoint by the same $\sigma\%$ from the baseline in the Emax model.

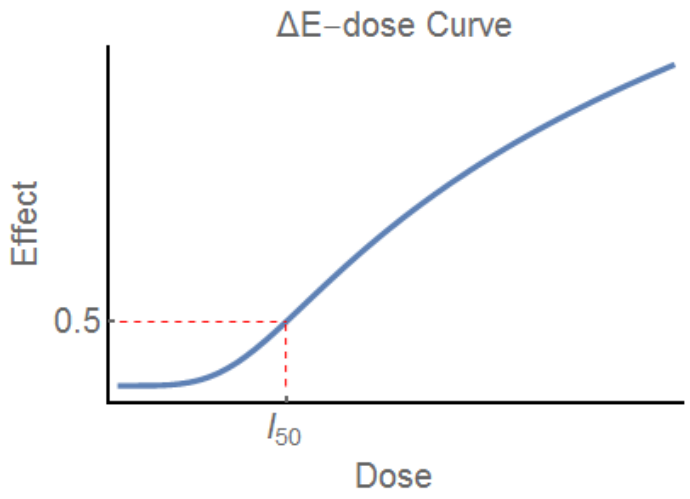

Figure 2.7: The $\Delta E - dose$ curve for the Exponential model.

In this chapter, we have introduced two different categories of model that describes the distribution of the medication inside the subject's body, namely PKPD model and DDDR model. We have shown that although the traditional PKPD model makes more intuitive sense in modeling the kinematics/dynamics of the drug, the lack of real-time plasma/blood drug concentration somewhat neutralizes this advantage and make it less attractive than the DDDR model. That is why we choose to use the DDDR model in the remaining chapters of this thesis. Then we introduced three models that describes the dose-response relationship of the drug, namely Emax model, Atan model and Exponential model. Among them, the Emax model is the most widely used model for the drugs that depress the endpoint [33].

However, when used to describe excitatory dose-response relationship, we are faced with the issue that maximum meaningful endpoint increase (E_{max}) is usually hard to determine. The remaining two models are proposed to get around this issue.

Chapter 3: System Identification and Sensitivity Analysis

3.1 Overview

In the previous chapter, we have presented two models (PKPD and DDDR model) to describe the drug distribution in the subject's body and three models (Emax, Atan and Exponential model) to describe the dose-response relationship of the drug. Due to the lack of real-time plasma/blood NE concentration, the PKPD model is not going to be considered here. In this chapter, we will validate and analyze these models by fitting the heart rate (HR) response of 5 piglets whose dataset comes from an animal experiment under the protocol approved by the Institutional Animal Care and Use Committee (IACUC) at the University of North Carolina, Chapel Hill. Each animal received NE at 5-6 distinct infusion rates of approximately 10 min duration under general anesthesia and mechanical ventilation to elicit a wide range of HR response. The minimum and maximum infusion rates used ranged between 0.05 mcg/kg/min and 0.5 mcg/kg/min, which resulted in a maximum HR response of 32-70 bpm, amounting to 22.1-64.8 % change from the baseline HR. All data are recorded using an 1 kHz sampling rate but is down-sampled to 10 Hz to lower the computational load. Besides, we also pre-process the HR measurements with an 15-point median filter to remove noise and outliers. The processed HR response of

these 5 pigs are shown in Fig. 3.1.

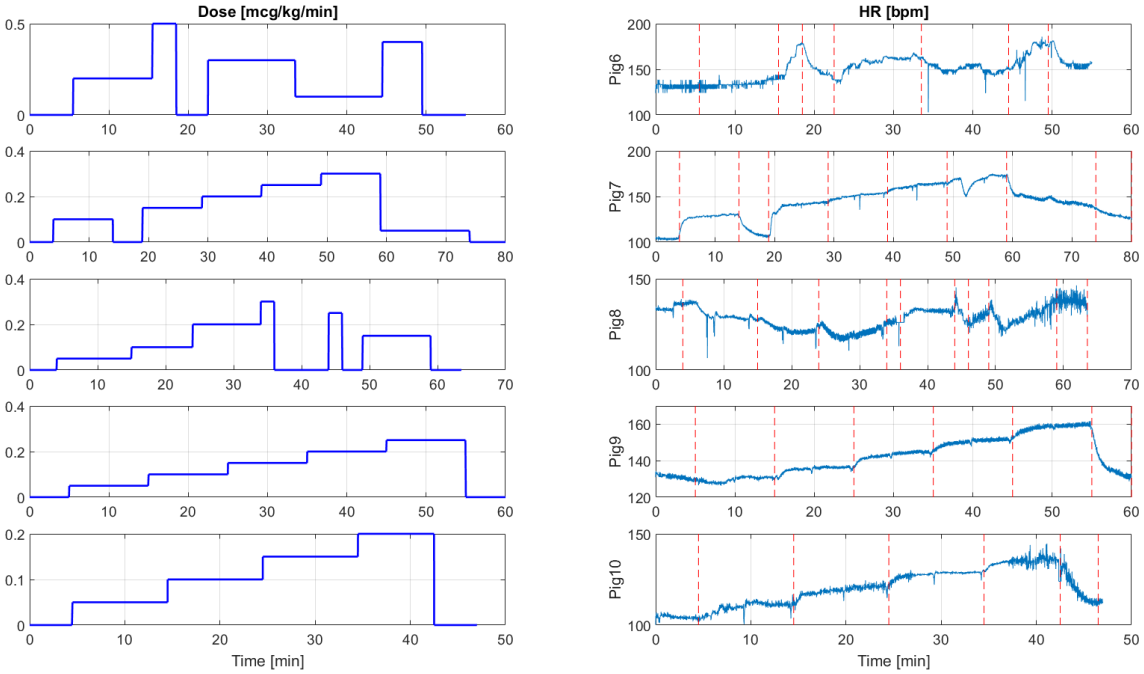

Figure 3.1: Heart rate dose-response of 5 pigs.

It should be noted that the HR response of pig 8 is very abnormal compared with other pigs, i.e., the HR response from 5-35 min decreases even though the dose level is actually increasing, which does not make sense. For this reason, the HR response of pig 8 is excluded from further analysis and only the remaining 4 pigs (namely, pig 6,7,9,10) are used. Besides, the HR response from 59 min to the end of pig 7 is far slower than the first 59 minutes of the data and is thus also excluded from the analysis.

3.2 System Identification

In this section we will perform system identification of the three models mentioned above by fitting the model to the experimental data associated with each

animal. More specifically, we will formulate and solve the following optimization problem using the numerical optimization tools available in MATLAB Optimization Toolbox [34]:

$$\theta^* = \arg\min_{\theta} ||\widetilde{R}(t) - R(t,\theta)|| \tag{3.1}$$

where θ^* is optimum value of θ minimizing the cost function (3.1), $\widetilde{R}(t)$ and $R(t,\theta)$ the measured versus model-predicted HR responses, where the model-predicted HR response was computed via pure (i.e., infinite-step-ahead) prediction. For the Atan and Exponential model we will examine the accuracy and parameters of the models identified with different values of σ. We will use the root-mean-squared error (RMSE) between measured versus model-predicted HR responses as the measure of accuracy.

3.2.1 Discretization

In the DDDR model, the drug distribution is governed by the following first-order system

$$\dot{I}_e(t) = -k_e I_e(t) + k_e u(t) \triangleq F(I_e(t)) \tag{3.2}$$

where $u(t)$ is the infusion dose level and $I_e(t)$ is the hypothetical effect site dose level. We discretize (3.2) as follows:

$$\frac{I_e(t) - I_e(t-1)}{h} = -k_e I_e(t) + k_e u(t) \;\Rightarrow\; I_e(t) = \frac{1}{1+k_e h} I_e(t-1) + h u(t) \tag{3.3}$$

where $h = 1/600$ min is the sampling interval. The dose-response relationship for the three models are discretized similarly using the backward difference scheme.

3.2.2 Emax Model

The Emax model has the following dose-response relationship:

$$R(t) = R_0 + R_m \frac{I_e^\lambda(t)}{I_e^\lambda(t) + I_{50}^\lambda} \triangleq H(I_e(t)) \tag{3.4}$$

where R_0 is the baseline HR, R_m the maximum therapeutically meaningful increase, $R(t)$ the medication HR response, $I_e(t)$ the effect site dose, I_{50} the dose required to reach half the effect of R_m and λ the Hill coefficient.

To investigate if this system is identifiable, the following matrix needs to have full column rank according to the identifiability rank condition [35]:

$$A = \begin{bmatrix} \frac{\partial L_F^0 H}{\partial I_e} & \frac{\partial L_F^0 H}{\partial k_e} & \frac{\partial L_F^0 H}{\partial R_m} & \frac{\partial L_F^0 H}{\partial I_{50}} & \frac{\partial L_F^0 H}{\partial \lambda} \\ \frac{\partial L_F^1 H}{\partial I_e} & \frac{\partial L_F^1 H}{\partial k_e} & \frac{\partial L_F^1 H}{\partial R_m} & \frac{\partial L_F^1 H}{\partial I_{50}} & \frac{\partial L_F^1 H}{\partial \lambda} \\ \frac{\partial L_F^2 H}{\partial I_e} & \frac{\partial L_F^2 H}{\partial k_e} & \frac{\partial L_F^2 H}{\partial R_m} & \frac{\partial L_F^2 H}{\partial I_{50}} & \frac{\partial L_F^2 H}{\partial \lambda} \\ \frac{\partial L_F^3 H}{\partial I_e} & \frac{\partial L_F^3 H}{\partial k_e} & \frac{\partial L_F^3 H}{\partial R_m} & \frac{\partial L_F^3 H}{\partial I_{50}} & \frac{\partial L_F^3 H}{\partial \lambda} \\ \frac{\partial L_F^4 H}{\partial I_e} & \frac{\partial L_F^4 H}{\partial k_e} & \frac{\partial L_F^4 H}{\partial R_m} & \frac{\partial L_F^4 H}{\partial I_{50}} & \frac{\partial L_F^4 H}{\partial \lambda} \end{bmatrix} \tag{3.5}$$

where L denotes the Lie derivative

$$L_F^0 H = H,\ L_F^1 H = \frac{\partial H}{\partial x} \cdot F,\ L_F^n H = L_F^1(L_F^{n-1} H),\ x = [I_e, k_e, R_m, I_{50}, \lambda] \tag{3.6}$$

Since the matrix A is extremely tedious, the column rank of the matrix is computed and verified using *Mathematica*:

The parameter constraints for different pigs are listed in Table. 3.1. The upper bound of R_m is set to roughly two times of the maximum increase observed across all 4 pigs.

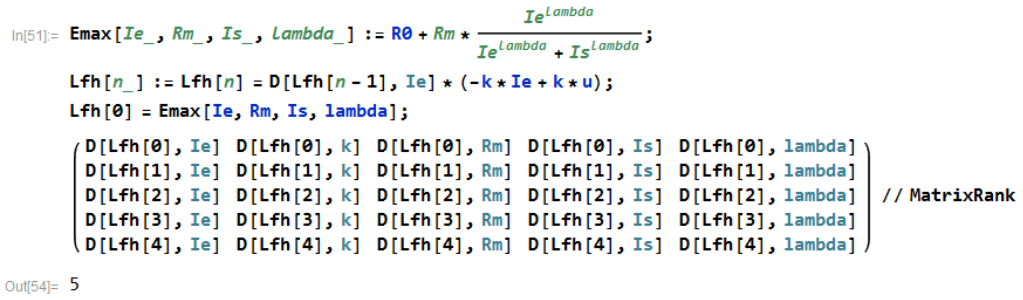

Figure 3.2: Computation of rank of the identifiability matrix for the Emax model.

	Pig 6	Pig 7	Pig 9	Pig 10
RMSE [bpm]	6.176	2.647	1.287	1.731

Table 3.2: RMSE of the fitted vs measured HR.

	k_e [min^{-1}]	R_0 [bpm]	R_m [bpm]	I_{50} [$mcg/kg/min$]	λ [N/A]
Pig 6	0.1-5.0	120.0-140.0	0-160.0	0-5.0	0-10.0
Pig 7	0.1-5.0	90.0-110.0	0-160.0	0-5.0	0-10.0
Pig 9	0.1-5.0	125.0-140.0	0-160.0	0-5.0	0-10.0
Pig 10	0.1-5.0	100.0-110.0	0-160.0	0-5.0	0-10.0

Table 3.1: Parameter bounds on 4 pigs with the Emax model.

The fitting result is shown in Fig. 3.3 and Table. 3.2 and the corresponding optimal parameters are listed in Table. 3.3.

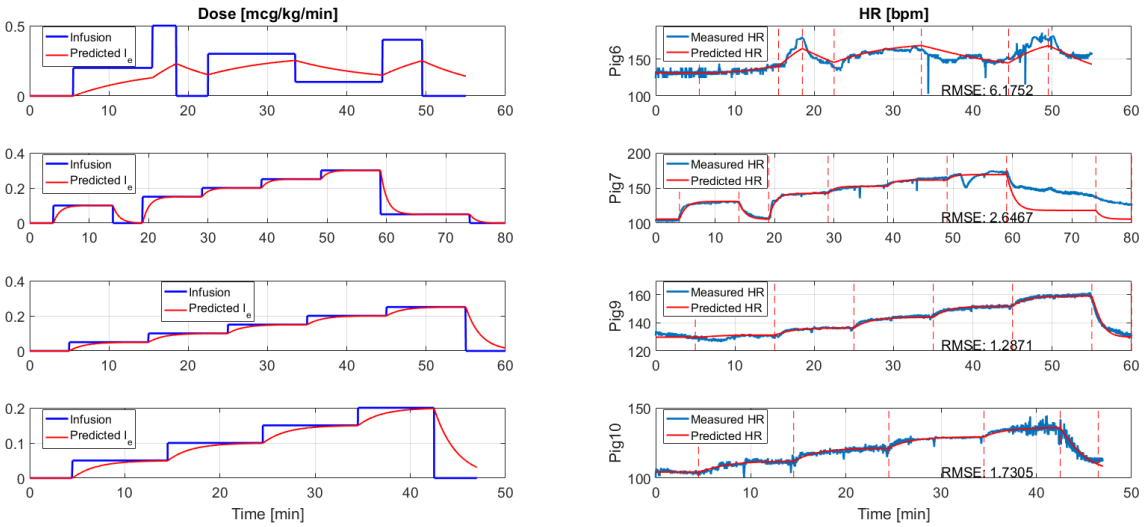

Figure 3.3: Predicted vs measured HR of the 4 pigs using the Emax model.

	k_e [min^{-1}]	R_0 [bpm]	R_m [bpm]	I_{50} [$mcg/kg/min$]	λ [N/A]
Pig 6	0.1050	131.5	52.90	0.2015	3.597
Pig 7	0.9387	105.7	160.0	0.4340	1.144
Pig 9	0.5400	129.8	57.19	0.2446	2.282
Pig 10	0.4157	104.3	70.66	0.2317	1.369

Table 3.3: Optimal parameters for the Emax model.

It should be noted that pig 7 never seems to actually achieve steady state, i.e., at the end of each dose level, the HR response is still increasing slightly, and thus it causes the parameter R_m to saturate. This will result in a biased estimate of other parameters for pig 7, however, we can do nothing about it.

3.2.3 Atan Model

The Atan model has the following dose-response relationship:

$$R(t) = R_0 + R_0 \times \sigma\% \times \tan\left(\frac{\pi}{2}\frac{I_e^\lambda}{I_e^\lambda + I_\sigma^\lambda}\right) \triangleq H(I_e(t)) \tag{3.7}$$

where R_0 is the baseline HR, $R(t)$ the medication HR response, $I_e(t)$ the effect site dose, I_σ the dose required to increase the HR by $\sigma\%$ of its baseline value and λ the Hill coefficient.

Again, in order for the system to be identifiable, the following matrix needs to have full column rank according to the identifiability rank condition [35]:

$$A = \begin{bmatrix} \frac{\partial L_F^0 H}{\partial I_e} & \frac{\partial L_F^0 H}{\partial k_e} & \frac{\partial L_F^0 H}{\partial I_\sigma} & \frac{\partial L_F^0 H}{\partial \lambda} \\ \frac{\partial L_F^1 H}{\partial I_e} & \frac{\partial L_F^1 H}{\partial k_e} & \frac{\partial L_F^1 H}{\partial I_\sigma} & \frac{\partial L_F^1 H}{\partial \lambda} \\ \frac{\partial L_F^2 H}{\partial I_e} & \frac{\partial L_F^2 H}{\partial k_e} & \frac{\partial L_F^2 H}{\partial I_\sigma} & \frac{\partial L_F^2 H}{\partial \lambda} \\ \frac{\partial L_F^3 H}{\partial I_e} & \frac{\partial L_F^3 H}{\partial k_e} & \frac{\partial L_F^3 H}{\partial I_\sigma} & \frac{\partial L_F^3 H}{\partial \lambda} \end{bmatrix} \tag{3.8}$$

where L denotes the Lie derivative

$$L_F^0 H = H,\ L_F^1 H = \frac{\partial H}{\partial x} \cdot F,\ L_F^n H = L_F^1(L_F^{n-1} H),\ x = [I_e, k_e, I_\sigma, \lambda] \tag{3.9}$$

Since the matrix A is extremely tedious, the column rank of the matrix is computed and verified using *Mathematica*:

The parameter constraints for different pigs are listed in Table. 3.4. Note that here we have used the same parameter constraints regardless of the σ value in the model.

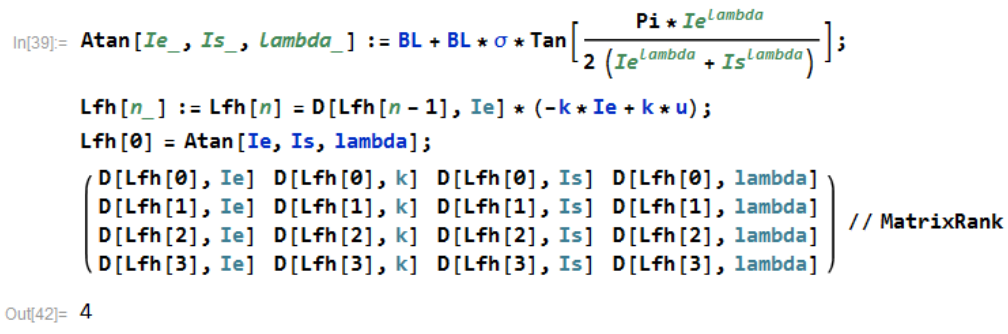

Figure 3.4: Computation of rank of the identifiability matrix for the Atan model.

	k_e [min^{-1}]	R_0 [bpm]	I_σ [$mcg/kg/min$]	λ [N/A]
Pig 6	0.1-5.0	90.0-110.0	0-5.0	0-10.0
Pig 7	0.1-5.0	90.0-110.0	0-5.0	0-10.0
Pig 9	0.1-5.0	125.0-140.0	0-5.0	0-10.0
Pig 10	0.1-5.0	100.0-110.0	0-5.0	0-10.0

Table 3.4: Parameter bounds on 4 pigs with the Atan model.

The fitting result is shown in Fig. 3.5 and Table. 3.5 and the corresponding optimal parameters are listed in Table. 3.6.

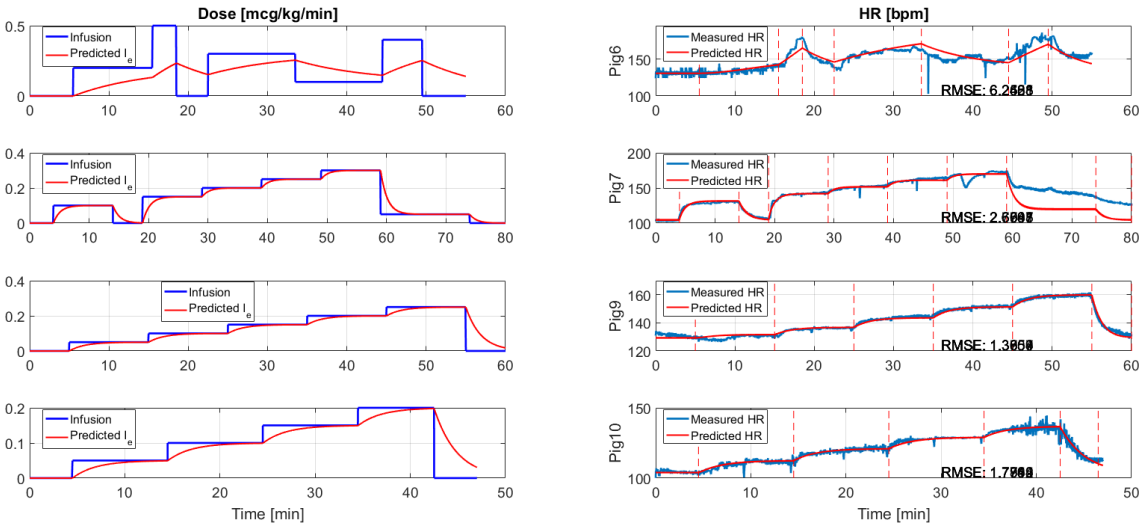

Figure 3.5: Predicted vs measured HR of the 4 pigs using the Atan model. Predicted HR using different σ are superimposed and plotted in the same figure.

RMSE [bpm]	Pig 6	Pig 7	Pig 9	Pig 10
$\sigma = 20$	6.261	2.701	1.366	1.780
$\sigma = 25$	6.254	2.700	1.360	1.785
$\sigma = 50$	6.246	2.679	1.371	1.771
$\sigma = 75$	6.249	2.664	1.385	1.775
$\sigma = 100$	6.252	2.657	1.396	1.780

Table 3.5: RMSE of the fitted vs measured HR.

		k_e [min^{-1}]	R_0 [bpm]	I_σ [$mcg/kg/min$]	λ [N/A]
Pig 6	$\sigma = 20$	0.1082	130.7	0.2029	2.361
	$\sigma = 25$	0.1080	130.7	0.2288	2.347
	$\sigma = 50$	0.1077	130.7	0.3381	2.215

	$\sigma = 75$	0.1077	130.7	0.4318	2.123
	$\sigma = 100$	0.1077	130.6	0.5158	2.067
Pig 7	$\sigma = 20$	0.8829	104.2	0.0697	0.9722
	$\sigma = 25$	0.8812	104.4	0.0944	0.9941
	$\sigma = 50$	0.8907	104.8	0.2296	1.023
	$\sigma = 75$	0.8984	104.9	0.3841	1.001
	$\sigma = 100$	0.9014	104.9	0.5610	0.9747
Pig 9	$\sigma = 20$	0.5307	129.4	0.2236	1.901
	$\sigma = 25$	0.5314	129.4	0.2600	1.872
	$\sigma = 50$	0.5307	129.3	0.4275	1.750
	$\sigma = 75$	0.5303	129.3	0.5803	1.684
	$\sigma = 100$	0.5300	129.3	0.7221	1.646
Pig 10	$\sigma = 20$	0.4156	103.9	0.1232	1.217
	$\sigma = 25$	0.4156	103.9	0.1556	1.210
	$\sigma = 50$	0.4157	104.0	0.3317	1.146
	$\sigma = 75$	0.4158	103.9	0.5316	1.100
	$\sigma = 100$	0.4158	103.9	0.7488	1.071

Table 3.6: Optimal parameters for the Atan model.

It should be noted that we did not optimize σ during the system identification process. Instead, we set $\sigma = 20/25/50/75/100$ and fit the models to the response

separately. From Table. 3.5 we see that changing σ in the model merely has an effect on the fitting. However, changing σ does influence the estimate of I_σ and λ as expected.

3.2.4 Exponential Model

The Exponential model has the following dose-response relationship:

$$R(t) = R_0 + \frac{R_0 \times \sigma\%}{\ln(1/3)} \times \ln\left(\frac{I_\sigma^\lambda}{2I_e^\lambda + I_\sigma^\lambda}\right) \triangleq H(I_e(t)) \tag{3.10}$$

where R_0 is the baseline HR, $R(t)$ the medication HR response, $I_e(t)$ the effect site dose, I_σ the dose required to increase the HR by $\sigma\%$ of its baseline value and λ the Hill coefficient.

Again, in order for the system to be identifiable, the following matrix needs to have full column rank according to the identifiability rank condition [35]:

$$A = \begin{bmatrix} \frac{\partial L_F^0 H}{\partial I_e} & \frac{\partial L_F^0 H}{\partial k_e} & \frac{\partial L_F^0 H}{\partial I_\sigma} & \frac{\partial L_F^0 H}{\partial \lambda} \\ \frac{\partial L_F^1 H}{\partial I_e} & \frac{\partial L_F^1 H}{\partial k_e} & \frac{\partial L_F^1 H}{\partial I_\sigma} & \frac{\partial L_F^1 H}{\partial \lambda} \\ \frac{\partial L_F^2 H}{\partial I_e} & \frac{\partial L_F^2 H}{\partial k_e} & \frac{\partial L_F^2 H}{\partial I_\sigma} & \frac{\partial L_F^2 H}{\partial \lambda} \\ \frac{\partial L_F^3 H}{\partial I_e} & \frac{\partial L_F^3 H}{\partial k_e} & \frac{\partial L_F^3 H}{\partial I_\sigma} & \frac{\partial L_F^3 H}{\partial \lambda} \end{bmatrix} \tag{3.11}$$

where L denotes the Lie derivative

$$L_F^0 H = H,\ L_F^1 H = \frac{\partial H}{\partial x} \cdot F,\ L_F^n H = L_F^1(L_F^{n-1} H),\ x = [I_e, k_e, I_\sigma, \lambda] \tag{3.12}$$

Since the matrix A is extremely tedious, the column rank of the matrix is computed and verified using *Mathematica*:

The parameter constraints for different pigs are listed in Table. 3.7. Note that

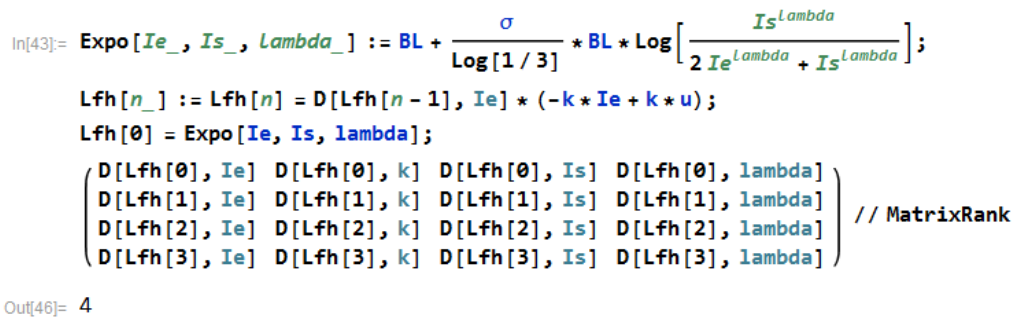

Figure 3.6: Computation of rank of the identifiability matrix for the Exponential model.

here we have used the same parameter constraints regardless of the σ value in the model.

	k_e [min^{-1}]	R_0 [bpm]	I_σ [$mcg/kg/min$]	λ [N/A]
Pig 6	0.1-5.0	90.0-110.0	0-5.0	0-10.0
Pig 7	0.1-5.0	90.0-110.0	0-5.0	0-10.0
Pig 9	0.1-5.0	125.0-140.0	0-5.0	0-10.0
Pig 10	0.1-5.0	100.0-110.0	0-5.0	0-10.0

Table 3.7: Parameter bounds on 4 pigs with the Exponential model.

The fitting result is shown in Fig. 3.7 and Table. 3.8 and the corresponding optimal parameters are listed in Table. 3.9.

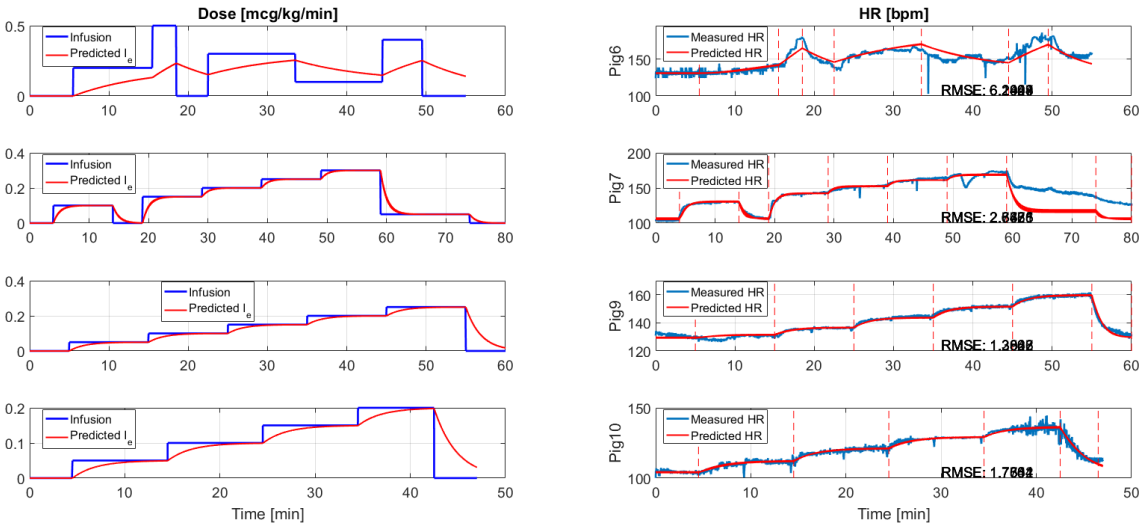

Figure 3.7: Predicted vs measured HR of the 4 pigs using the Exponential model. Predicted HR using different σ are superimposed and plotted in the same figure.

RMSE [bpm]	Pig 6	Pig 7	Pig 9	Pig 10
$\sigma = 20$	6.196	2.837	1.286	1.736
$\sigma = 25$	6.205	2.777	1.303	1.733
$\sigma = 50$	6.231	2.669	1.356	1.750
$\sigma = 75$	6.243	2.648	1.381	1.765
$\sigma = 100$	6.249	2.643	1.395	1.774

Table 3.8: RMSE of the fitted vs measured HR.

		k_e [min^{-1}]	R_0 [bpm]	I_σ [$mcg/kg/min$]	λ [N/A]
Pig 6	$\sigma = 20$	0.1066	131.1	0.2018	3.019
	$\sigma = 25$	0.1068	131.0	0.2289	2.768
	$\sigma = 50$	0.1073	130.7	0.3536	2.291

	$\sigma = 75$	0.1075	130.7	0.4610	2.141
	$\sigma = 100$	0.1077	130.6	0.5559	2.067
Pig 7	$\sigma = 20$	1.053	107.1	0.0946	2.072
	$\sigma = 25$	1.013	106.8	0.1123	1.787
	$\sigma = 50$	0.9415	105.9	0.2359	1.260
	$\sigma = 75$	0.9221	105.4	0.4076	1.099
	$\sigma = 100$	0.9140	105.2	0.6178	1.022
Pig 9	$\sigma = 20$	0.5366	129.7	0.2249	2.199
	$\sigma = 25$	0.5346	129.6	0.2659	2.054
	$\sigma = 50$	0.5312	129.4	0.4602	1.775
	$\sigma = 75$	0.5304	129.3	0.6358	1.685
	$\sigma = 100$	0.5300	129.3	0.7969	1.642
Pig 10	$\sigma = 20$	0.4154	104.4	0.1232	1.5663
	$\sigma = 25$	0.4155	104.3	0.1569	1.437
	$\sigma = 50$	0.4157	104.0	0.3616	1.189
	$\sigma = 75$	0.4158	103.9	0.6026	1.110
	$\sigma = 100$	0.4158	103.9	0.8646	1.072

Table 3.9: Optimal parameters for the Exponential model.

It should be noted that we did not optimize σ during the system identification

process. Instead, we set $\sigma = 20/25/50/75/100$ and fit the models to the response separately. From Table. 3.8 we see that changing σ in the model merely has an effect on the fitting. However, changing σ does influence the estimate of I_σ and λ as expected.

3.3 Sensitivity Analysis

In this section, we will perform sensitivity analysis using the above-mentioned three models to determine the relative importance of the parameters in each model. As we will mention in detail in Chapter 4.2, we specifically want to see that λ has the least sensitivity so that we can fix λ at its nominal value in the controller settings. The parameter sensitivity function is calculated using the formula in Khalil's "Nonlinear Systems" [36].

3.3.1 Emax Model

For the Emax model, the parameter set is $\theta = [k_e, R_0, R_m, I_{50}, \lambda]^T$. However, we are only interested in the sensitivity of k_e, I_{50} and λ. Using eqs. (3.2) and (3.4), the sensitivity function is given by

$$\dot{S}_{I_e}(t) = \frac{\partial F}{\partial I_e} S_{I_e(t)} + \frac{\partial F}{\partial \theta} = -k_e S_{I_e}(t) + \begin{bmatrix} u(t) - I_e(t) \\ 0 \\ 0 \end{bmatrix} \tag{3.13a}$$

$$S_R(t) = \frac{\partial H}{\partial I_e} S_{I_e}(t) + \frac{\partial H}{\partial \theta}$$

$$= \frac{R_0 \lambda I_{50}^{\lambda} I_e^{\lambda-1}(t)}{(I_{50}^{\lambda} + I_e^{\lambda}(t))^2} S_{I_e}(t) + \begin{bmatrix} 0 \\ -\frac{R_0 \lambda I_{50}^{\lambda-1} I_e^{\lambda}(t)}{(I_{50}^{\lambda}+I_e^{\lambda}(t))^2} \\ -\frac{R_0 I_{50}^{\lambda}(\ln I_{50} - \ln I_e(t)) I_e^{\lambda}(t)}{(I_{50}^{\lambda}+I_e^{\lambda}(t))^2} \end{bmatrix} \tag{3.13b}$$

where $S_{I_e}(t) = \left[\frac{\partial I_e(t)}{\partial k_e}, \frac{\partial I_e(t)}{\partial I_\sigma}, \frac{\partial I_e(t)}{\partial \lambda}\right]^T$, $S_R(t) = \left[\frac{\partial R(t)}{\partial k_e}, \frac{\partial R(t)}{\partial I_\sigma}, \frac{\partial R(t)}{\partial \lambda}\right]^T$, and $\theta = \left[k_e, I_{50}, \lambda\right]^T$. Considering that $\lim_{t\to\infty} \frac{\partial I_e(t)}{\partial I_\sigma} = 0$ and $\lim_{t\to\infty} \frac{\partial I_e(t)}{\partial \lambda} = 0$, (3.13b) reduces to the following:

$$S_R(t) \to \begin{bmatrix} \frac{R_0 \lambda I_{50}^{\lambda} I_e^{\lambda-1}(t)}{(I_{50}^{\lambda}+I_e^{\lambda}(t))^2} \frac{\partial I_e(t)}{\partial k_e} \\ -\frac{R_0 \lambda I_{50}^{\lambda-1} I_e^{\lambda}(t)}{(I_{50}^{\lambda}+I_e^{\lambda}(t))^2} \\ -\frac{R_0 I_{50}^{\lambda}(\ln I_{50} - \ln I_e(t)) I_e^{\lambda}(t)}{(I_{50}^{\lambda}+I_e^{\lambda}(t))^2} \end{bmatrix} \tag{3.14}$$

with $\frac{\partial I_e(t)}{\partial k_e} = \int_0^t e^{-k_e(t-\tau)}[u(\tau) - I_e(\tau)]\, d\tau$. The sensitivity plot is shown in Fig. 3.8.

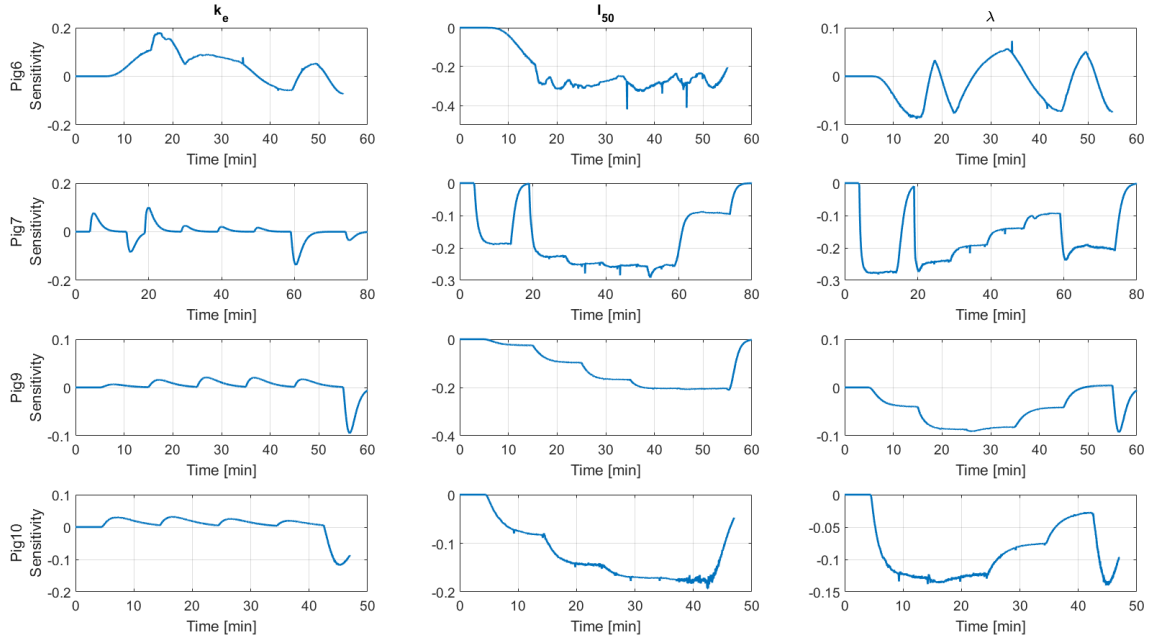

Figure 3.8: Sensitivity of the parameters using the Emax model.

3.3.2 Atan Model

For the Atan model, the parameter set is $\theta = [k_e, R_0, I_\sigma, \lambda]^T$. However, we are only interested in the sensitivity of k_e, I_σ and λ. Using eqs. (3.2) and (3.7), the sensitivity function is given by

$$\dot{S}_{I_e}(t) = \frac{\partial F}{\partial I_e} S_{I_e(t)} + \frac{\partial F}{\partial \theta} = -k_e S_{I_e}(t) + \begin{bmatrix} u(t) - I_e(t) \\ 0 \\ 0 \end{bmatrix} \tag{3.15a}$$

$$\begin{aligned} S_R(t) &= \frac{\partial H}{\partial I_e} S_{I_e}(t) + \frac{\partial H}{\partial \theta} \\ &= \frac{R_0 \sigma \lambda I_\sigma^\lambda I_e^{\lambda-1}(t) \pi \csc^2(p)}{2(I_\sigma^\lambda + I_e^\lambda(t))^2} S_{I_e}(t) + \begin{bmatrix} 0 \\ -\frac{R_0 \sigma \lambda I_\sigma^{\lambda-1} I_e^\lambda(t) \pi \csc^2(p)}{2(I_\sigma^\lambda + I_e^\lambda(t))^2} \\ -\frac{R_0 \sigma I_\sigma^\lambda (\ln I_\sigma - \ln I_e(t)) I_e^\lambda(t) \pi \csc^2(p)}{2(I_\sigma^\lambda + I_e^\lambda(t))^2} \end{bmatrix} \end{aligned} \tag{3.15b}$$

where

$$p = \frac{I_\sigma^\lambda}{2(I_\sigma^\lambda + I_e^\lambda(t))} \tag{3.16}$$

and $S_{I_e}(t) = \left[\frac{\partial I_e(t)}{\partial k_e}, \frac{\partial I_e(t)}{\partial I_\sigma}, \frac{\partial I_e(t)}{\partial \lambda}\right]^T$, $S_R(t) = \left[\frac{\partial R(t)}{\partial k_e}, \frac{\partial R(t)}{\partial I_\sigma}, \frac{\partial R(t)}{\partial \lambda}\right]^T$, and $\theta = \left[k_e, I_\sigma, \lambda\right]^T$. Considering that $\lim_{t\to\infty} \frac{\partial I_e(t)}{\partial I_\sigma} = 0$ and $\lim_{t\to\infty} \frac{\partial I_e(t)}{\partial \lambda} = 0$, (3.15b) reduces to the following:

$$S_R(t) \to \begin{bmatrix} \frac{R_0 \sigma \lambda I_\sigma^\lambda I_e^{\lambda-1}(t) \pi \csc^2(p)}{2(I_\sigma^\lambda + I_e^\lambda(t))^2} \frac{\partial I_e(t)}{\partial k_e} \\ -\frac{R_0 \sigma \lambda I_\sigma^{\lambda-1} I_e^\lambda(t) \pi \csc^2(p)}{2(I_\sigma^\lambda + I_e^\lambda(t))^2} \\ -\frac{R_0 \sigma I_\sigma^\lambda (\ln I_\sigma - \ln I_e(t)) I_e^\lambda(t) \pi \csc^2(p)}{2(I_\sigma^\lambda + I_e^\lambda(t))^2} \end{bmatrix} \tag{3.17}$$

with $\frac{\partial I_e(t)}{\partial k_e} = \int_0^t e^{-k_e(t-\tau)}[u(\tau) - I_e(\tau)]\, d\tau$. The sensitivity plot is shown in Fig. 3.9.

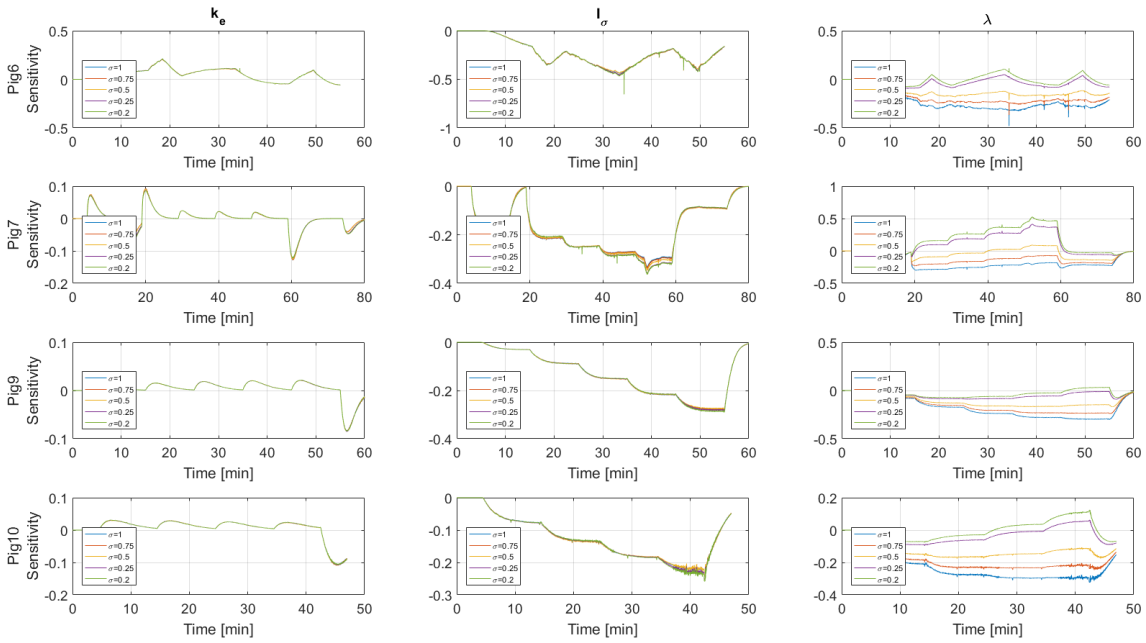

Figure 3.9: Sensitivity of the parameters using the Atan model.

3.3.3 Exponential Model

For the Exponential model, the parameter set is $\theta = [k_e, R_0, I_\sigma, \lambda]^T$. However, we are only interested in the sensitivity of k_e, I_σ and λ. Using eqs. (3.2) and (3.10), the sensitivity function is given by

$$\dot{S}_{I_e}(t) = \frac{\partial F}{\partial I_e} S_{I_e(t)} + \frac{\partial F}{\partial \theta} = -k_e S_{I_e}(t) + \begin{bmatrix} u(t) - I_e(t) \\ 0 \\ 0 \end{bmatrix} \tag{3.18a}$$

$$\begin{aligned} S_R(t) &= \frac{\partial H}{\partial I_e} S_{I_e}(t) + \frac{\partial H}{\partial \theta} \\ &= \frac{R_0 \sigma}{\ln(3)} \frac{2\lambda I_e^{\lambda-1}(t)}{I_\sigma^\lambda + 2I_e^\lambda(t)} S_{I_e}(t) + \begin{bmatrix} 0 \\ -\frac{R_0\sigma}{\ln(3) I_\sigma} \frac{2\lambda I_e^\lambda(t)}{I_\sigma^\lambda + 2I_e^\lambda(t)} \\ -\frac{R_0\sigma}{\ln(3)} \frac{2(\ln I_\sigma - \ln I_e(t)) I_e^\lambda(t)}{I_\sigma^\lambda + 2I_e^\lambda(t)} \end{bmatrix} \end{aligned} \tag{3.18b}$$

where $S_{I_e}(t) = \left[\frac{\partial I_e(t)}{\partial k_e}, \frac{\partial I_e(t)}{\partial I_\sigma}, \frac{\partial I_e(t)}{\partial \lambda}\right]^T$, $S_R(t) = \left[\frac{\partial R(t)}{\partial k_e}, \frac{\partial R(t)}{\partial I_\sigma}, \frac{\partial R(t)}{\partial \lambda}\right]^T$, and $\theta = \left[k_e, I_\sigma, \lambda\right]^T$. Considering that $\lim_{t\to\infty} \frac{\partial I_e(t)}{\partial I_\sigma} = 0$ and $\lim_{t\to\infty} \frac{\partial I_e(t)}{\partial \lambda} = 0$, (3.18b) reduces to the following:

$$S_R(t) \to \begin{bmatrix} \frac{R_0\sigma}{\ln(3)} \frac{2\lambda I_e^{\lambda-1}(t)}{I_\sigma^\lambda + 2I_e^\lambda(t)} \frac{\partial I_e(t)}{\partial k_e} \\ -\frac{R_0\sigma}{\ln(3) I_\sigma} \frac{2\lambda I_e^\lambda(t)}{I_\sigma^\lambda + 2I_e^\lambda(t)} \\ -\frac{R_0\sigma}{\ln(3)} \frac{2(\ln I_\sigma - \ln I_e(t)) I_e^\lambda(t)}{I_\sigma^\lambda + 2I_e^\lambda(t)} \end{bmatrix} \tag{3.19}$$

with $\frac{\partial I_e(t)}{\partial k_e} = \int_0^t e^{-k_e(t-\tau)}[u(\tau) - I_e(\tau)]\, d\tau$. The sensitivity plot is shown in Fig. 3.10.

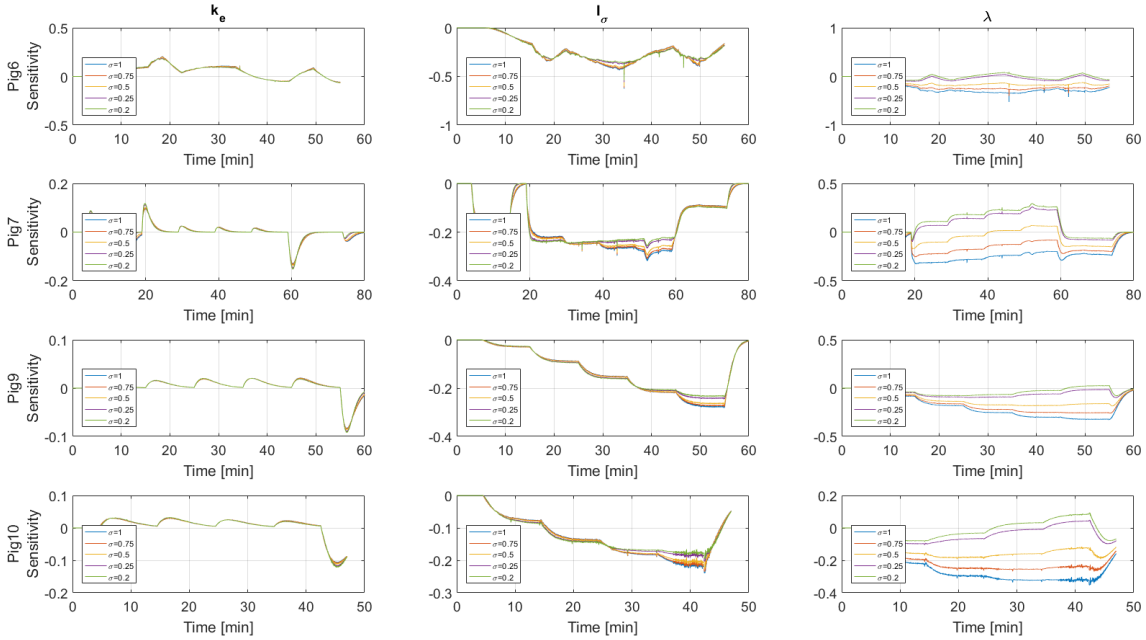

Figure 3.10: Sensitivity of the parameters using the Exponential model.

3.4 Discussion

3.4.1 More on Exponential Model

As mentioned earlier, we want λ to have the least sensitivity compared with k_e and I_σ/I_{50} so that we can fix λ at its nominal value in the controller and thus to enable linear parametrization (see Chapter 4.2). From the results we obtained above, it can be seen that for the Emax model the magnitude ratio between the sensitivity of $R(t)$ to k_e versus λ and I_{50} versus λ are given by:

$$\begin{aligned}\left|\frac{S_{R,k_e}(t)}{S_{R,\lambda}(t)}\right| &\to \frac{\lambda}{I_e(\ln I_{50} - \ln I_e(t))}\frac{\partial I_e(t)}{\partial k_e} \\ \left|\frac{S_{R,I_e}(t)}{S_{R,\lambda}(t)}\right| &\to \frac{\lambda}{I_{50}(\ln I_{50} - \ln I_e(t))}\end{aligned} \tag{3.20}$$

while for the Atan and Exponential model

$$\begin{aligned}\left|\frac{S_{R,k_e}(t)}{S_{R,\lambda}(t)}\right| &\to \frac{\lambda}{I_e(\ln I_\sigma - \ln I_e(t))}\frac{\partial I_e(t)}{\partial k_e} \\ \left|\frac{S_{R,I_e}(t)}{S_{R,\lambda}(t)}\right| &\to \frac{\lambda}{I_\sigma(\ln I_\sigma - \ln I_e(t))}\end{aligned} \tag{3.21}$$

Ideally, these two ratios should be as large as possible, i.e., the models sensitivity to λ must be negligible relative to k_e and I_σ/I_{50} [31]. However for the Emax model, since we do not know the relative magnitude of $I_e(t)$ and I_{50} before hand, it is impossible to reliably guarantee that these ratios are going to be large and thus making it less legitimate to use population averaged value for λ in the controller settings. But for Atan and Exponential model, given that both ratios in (3.21) are infinite if $I_\sigma = I_e(t)$ (assuming that $\frac{\partial I_e(t)}{\partial k_e} \neq 0$, which is always satisfied during transients), one way to fulfill the requirements in (3.21) is to set I_σ as the value

of $I_e(t)$ in the steady state. This can be easily achieved, for example, by setting σ consistently with the control set point (i.e., if the set point associated with $R(t)$ is σ^* % increase from R_0, set $\sigma = \sigma^*$).

At this point with the results from the system identification and sensitivity analysis, we can compare the pros and cons of the Emax model, Atan model and Exponential model with more confidence. The Emax model is inarguably the most popular model [33], but it faces the difficulties that either E_{max} is hard to determine for individual subject or that if it is fixed at the therapeutically allowed maximum value, we run the risk of having the experiment doses almost entirely in the sub-maximal region and thus endangering the estimate of I_{50}. The Atan and Exponential model however, get around these issues by allowing the endpoints to go to infinity (although it never will in the real world) and by setting the σ parameter in accordance with the desired target point. The introduction of σ also brings along another advantage, i.e., the sensitivity of λ is the least compared with k_e and I_σ at the steady state. Combined with the fact that the steady state is usually much longer than the transient state in the actual clinical settings, it makes the choice to use population averaged λ in the controller more legitimate. Within the Atan and Exponential model, the dose-response curve for the Atan model approaches a vertical line (i.e., the subject responds more and more violently with increasing dose) which does not make physiological sense. The Exponential model, in contrast, has a very similar three-phase dose-response curve as the Emax model. In particular, since the derivative of the natural log function approaches zero at the end, marginal dose effect is going to decrease when the dose is very large which resembles the

Emax model. Despite all the aforementioned advantages, the Exponential model still have one disadvantage, i.e., since the dose-response curve of the Exponential model assumes no upper bound whereas the Emax model does have one, the Exponential model can only mimic the behavior up to a certain dose level. However, this is compensated by the fact that (1) the estimated HR from the Exponential model is the same as that from the Emax model at the steady state and (2) the transient tracking error can be alleviated by using larger controller gains.

3.4.2 Accuracy of Parameter Estimation

The results of the system identification analysis (see Table. 3.8) using experimental data showed that the Exponential model could reproduce experimental dose-response relationship accurately regardless of the choice of σ (Fig. 3.11; also see the consistency in the RMSE values against different σ values in Table. 3.10). In addition, the estimated model parameters were plausible. Specifically, we anticipated that I_σ value would be estimated to be proportional to σ due to its definition, while k_e and λ values would be independent of σ. Table. 3.10 clearly shows these anticipated trends: on the average, the variability in k_e and λ with respect to σ was small, while I_σ exhibited a much larger variability with a proportionally increasing trend with σ, which is consistent with the notion that I_σ designates the infusion rate corresponding to σ % increase in response from the baseline.

Fig. 3.12 compares I_σ values obtained directly from experimental data versus estimated from system identification. We extracted the former from the experimen-

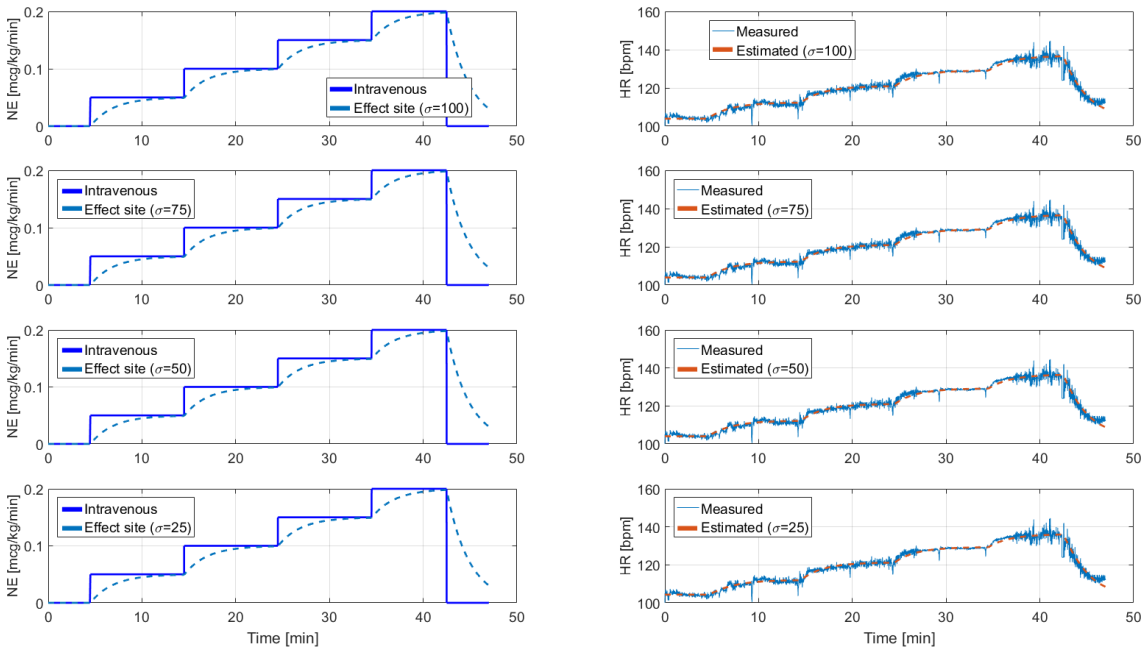

Figure 3.11: Representative example of intravenous versus model-predicted hypothetical effect site norepinephrine (NE) infusion rates (left), and the resulting measured versus model-predicted heart rate (HR) responses (right) in an animal.

	RMSE [bpm]	k_e [min^{-1}]	I_σ [mcg/kg/min]	λ [·]
$\sigma = 25$	1.3-6.2	0.11-1.0	0.11-0.27	1.4-2.8
$\sigma = 50$	1.3-6.2	0.11-0.94	0.24-0.46	1.2-2.3
$\sigma = 75$	1.4-6.2	0.11-0.92	0.41-0.64	1.1-2.1
$\sigma = 100$	1.4-6.2	0.11-0.91	0.56-0.87	1.0-2.1

Table 3.10: Root-mean-squared prediction errors (RMSEs) and the range of model parameter values associated with all animals with respect to σ.

tal data by (i) computing the % increase in HR at the end of each step infusion dose (e.g., 0.05, 0.1, 0.15, and 0.2 mcg/kg/min in Fig. 3.11; % increase was computed as the average of the last 1 minute associated with each infusion dose), (ii) denoting the % increase in HR associated with each infusion dose as σ, and (iii) defining I_σ as the corresponding step infusion dose (e.g., 0.05 mcg/kg/min in Fig. 3.11 was defined as I_6, because it resulted in 6 % increase in HR). Overall, measured and estimated I_σ values were consistent in all animals, which supports quantitatively the validity of the dose-response model derived from the system identification (except in pig 6, in which the medication distribution dynamics was slow ($k_e = 0.11\,\text{min}^{-1}$, corresponding to a 2 % settling time of 35.6 min) and steady state was not reached within the step infusion duration of 10 min). The other explanation to the defect in Pig 6 may be that the HR response during 5-15 min is lower than expected for some unknown reason since the HR during this period is almost lower than HR during all the other dose levels (as shown in Fig. 3.7) whereas the dose level corresponding to this period (0.2 mcg/kg/min) is not. If we exclude this portion of the data in the fitting process, i.e., the fitting error is this portion of the data is not considered in minimizing the cost function (3.1), the result is shown in Fig. 3.13 and average fitting error reduces from around 6.2 bpm to around 5.8 bpm. It can be seen that the I_σ estimates from both sources agree better than before. However, this does not necessarily means that this explanation is preferred over the previous one. Instead we simply observe the defect between the measured data and estimated response and propose reasonable causes that account for the discrepancy, and more rigorous reasoning should come from further animal experiments.

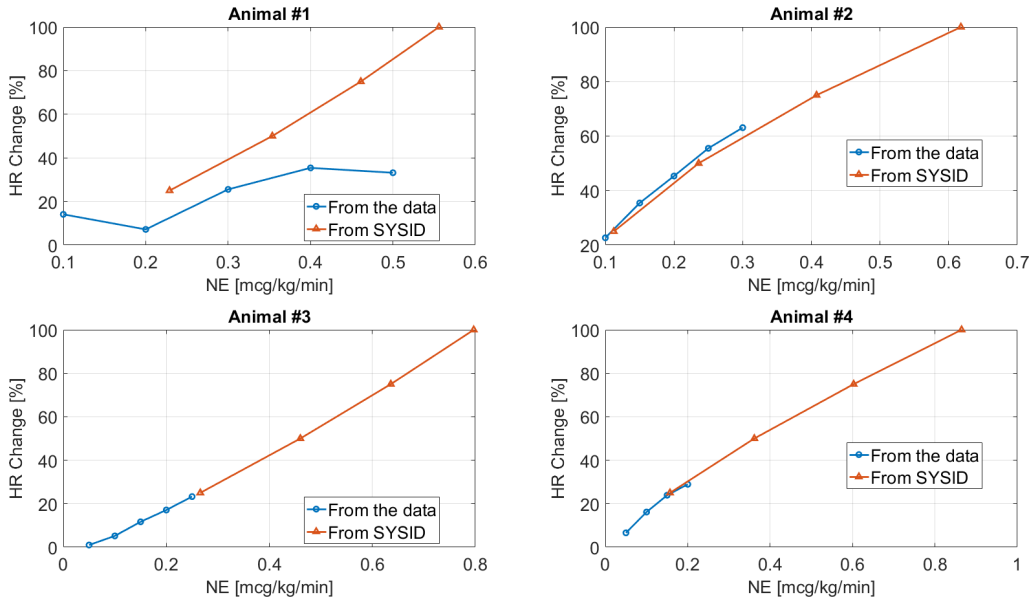

Figure 3.12: Comparison of I_σ values obtained directly from experimental data (circle) versus estimated from system identification (triangle).

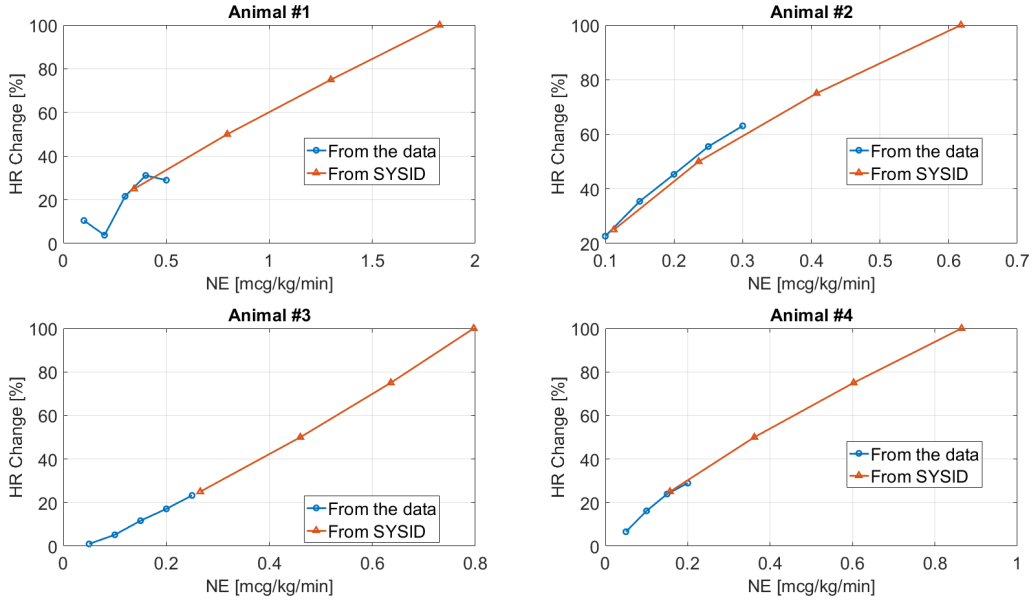

Figure 3.13: Comparison of I_σ values obtained directly from experimental data (circle) versus estimated from system identification (triangle) with a portion of the data in Pig 6 excluded from system identification process.

Considering that the traditional Emax model and the Exponential model are different in terms of the way the steady-state infusion dose parameter is specified, the ability to estimate I_σ accurately is a meaningful strength of the Exponential model. The former specifies $I_{50}^{E_{max}}$ with respect to the maximum response, whereas the latter specifies I_σ with respect to the baseline response. Thus, the accuracy of $I_{50}^{E_{max}}$ is subject to compromise in case the maximum response is inadequately estimated (which is highly probable in real clinical settings now that it is extremely challenging to estimate the maximum response in the absence of response data associated with very high infusion dose regimes). In contrast, the accuracy of I_σ is easier to guarantee because the baseline response is almost always available.

Although the accuracy and parametric plausibility of the Exponential model were shown to be robust against the choice of σ, it is not clear what is the best choice of σ to maximize its amenity to control design and system identification. Considering that parametric accuracy is an important requirement for system identification, it is desired that the model parameters (especially I_σ which dictates the models steady-state validity) is accurately estimated. Thus, we want to investigate the parametric accuracy of the Exponential model with respect to the infusion rate amplitude and the value of σ. Of particular interest was to gain insights as to how to set the value of σ when an infusion rate input is given in order to maximize the accuracy of I_σ. To this end, we constructed a ground truth Emax model (3.22), where $\bar{R}_0$, $\bar{k}_e$, $\bar{I}_{50}^{E_{max}}$, and $\bar{\lambda}$ denote nominal (i.e., average) parameters obtained from the system identification of the Emax model in all the animals, and $\bar{R}_m$ the maximum possible change in response (specified as twice the maximum change in response across all

the animals):

$$\dot{I}_e(t) = -\bar{k}_e I_e(t) + \bar{k}_e u(t), \qquad R(t) = \bar{R}_0 + \bar{R}_m \frac{I_e^{\bar{\lambda}}(t)}{I_e^{\bar{\lambda}}(t) + \left(\bar{I}_{50}^{E_{max}}\right)^{\bar{\lambda}}} \tag{3.22}$$

Note that $\bar{I}_{50}^{E_{max}}$ in (3.22) denotes the steady-state infusion rate to elicit 50% of maximum response $\bar{R}_m$. Then, we simulate the ground truth Emax model with a set of infusion rate inputs to generate input-output data pairs, and identify the Exponential model associated with each input-output data pair. We specifically employed 3 step infusion rate inputs to simulate the ground truth model, with the maximum rates corresponding to 25%, 50%, and 75% increases in response relative to the baseline. In identifying the Exponential model for each input-output data pair, we used $\sigma = 20, 25, 50, 75, 100$. Then, we examined the accuracy of the identified I_σ values.

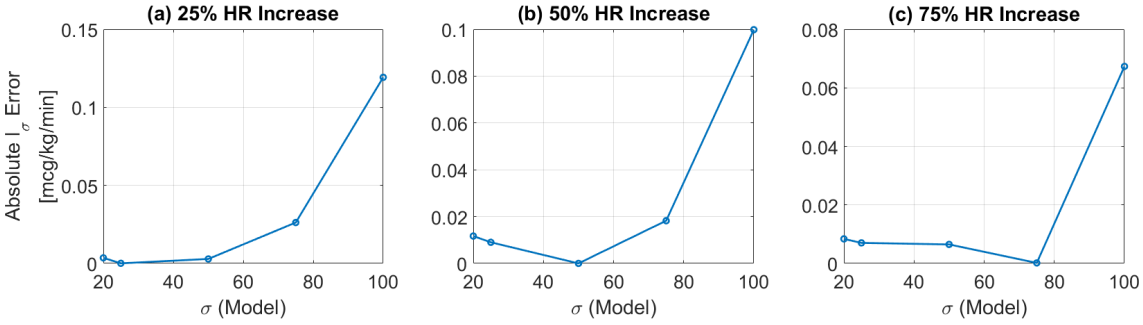

Figure 3.14: Estimation error associated with I_σ of model M_σ, $\sigma = 20, 25, 50, 75, 100$ when subject to 25 %, 50 %, and 75 % step increase in HR. (a) 25 % HR increase. (b) 50 % HR increase. (c) 75 % HR increase.

Fig. 3.14 shows that the error associated with I_σ estimated from step response system identification is minimized when σ is set to the actual steady-state % change in the systems response. These results suggest that semi-adaptive control may bene-

fit from setting σ consistently to the specified target set point (i.e., the % difference between the baseline state and target), by minimizing the unwanted influence of λ on control efficacy as well as estimation error on I_σ. Note that σ may be reset recursively, e.g., each time the target set point is varied by the caregiver.

3.4.3 Tuning the Sensitivity

In Chapter 3.4.1, we have proven that the sensitivity of the Exponential model to λ relative to k_e and I_σ can be made small by specifying σ in the model as the percent change in response induced by the infusion rate inputted to the model. To verify this, we constructed nominal dose-response models, denoted as M_σ, relating NE infusion rate to HR associated with different values of σ based on the dose-response models obtained from system identification (Table. 3.3). We specifically considered $\sigma = 25, 50, 75, 100$. Then, we excited each M_σ using 4 step inputs eliciting 25 %, 50 %, 75 %, and 100 % change in HR, and examined the time evolution of the parametric sensitivity functions (3.18). In particular, we compared the relative magnitudes of the parametric sensitivity functions across all the 4 nominal models for each step infusion rate input to examine if the models sensitivity to λ is the smallest when σ used in the model is consistent with the input applied to the model. Fig. 3.15 shows that the sensitivity of the response to λ can be made zero (after initial transient) by setting the value of σ incorporated in the Exponential model (3.10) to the actual % change in response.

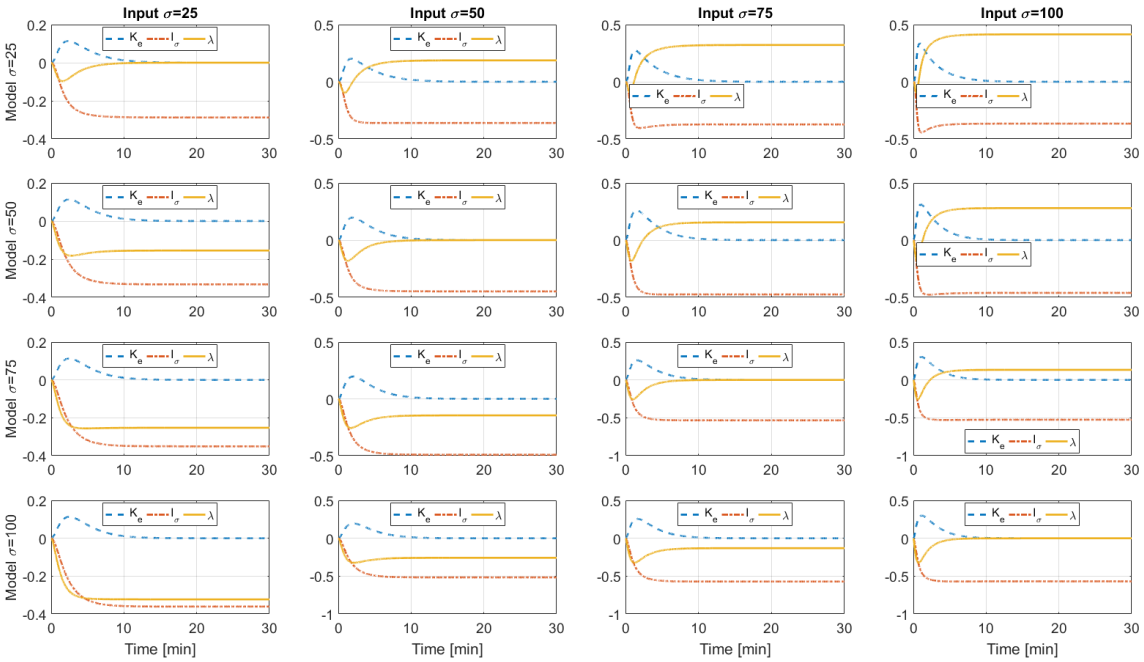

Figure 3.15: Time evolution of parametric sensitivity functions associated with models M_σ, $\sigma = 25, 50, 75, 100$. (a) 25 % HR increase. (b) 50 % HR increase. (c) 75 % HR increase. (d) 100 % HR increase.

For all of the reasons above, we are going to use Exponential model (combing with the DDDR model) to describe the full dose-response relationship of NE and implement the model into the controller in the following chapter.

Chapter 4: Semi-Adaptive Closed-Loop Controller Design

4.1 Overview

Closed-loop control of medication infusion has been an active field of research for a few decades in critical care medicine, with a large number of work reported on closed-loop control of anesthesia, analgesia, and neuromuscular blockade [9–12]. These medications commonly exhibit depressive dose-dependent effects, often with minimum possible response of zero. For example, propofol depresses the degree of consciousness, which is measured by indices such as BIS ranging between 100 (fully awake) and 0 (fully asleep) [37]. Remifentanil depresses respiratory rate, also ranging between its nominal value (when not infused) and zero (in case overdosed) [38, 39]. The boundedness of the range of response with its explicit upper (baseline) and lower (zero) limits facilitated the use of classical dose-response models, e.g., the Emax model [20], in designing closed-loop controllers for infusion of these medications (see, e.g., [18, 21–28]).

In contrast to the above, medications such as vasopressors and inotropes exhibit excitatory dose-dependent effects. A unique challenge associated with closed-loop control of such medications is that the upper limit of medication-induced excitatory response (a parameter that must be specified to characterize the Emax

model) is unknown. In fact, it is extremely difficult, if not impossible, to determine the upper limit of response in a patient in real clinical settings due to patient safety and ethical considerations. A conceivable alternative may be to estimate the upper limit via advanced control techniques, e.g., adaptive control. However, given that the infusion rate may mostly reside in sub-maximal dose regime (where desired effect is maximized while dangerous side effects are prevented), the credibility of estimated upper response limit (and accordingly, other parameters in the model influenced by the upper response limit) is expected to be low due to the rare incidence of appropriate dose-response data in the neighborhood of maximal dose regime. Despite this prominent challenge, there has not been rigorous research effort to establish model-based closed-loop control techniques for infusion of these medications. In fact, most existing work employ empiric model-free techniques such as PID, fuzzy logic, and rule-based techniques [40–42].

In an attempt to address this challenge, we present a semi-adaptive closed-loop control approach to infusion of medications that exhibit excitatory dose-dependent effects. We developed a new dose-response model (the Exponential model, as mentioned in the previous chapters) by extending a classical dose-response model (the Emax model) used for medications with depressive effects by a nonlinear transformation, and extended a semi-adaptive control approach developed in our prior work [31], applicable to depressive dose-response relationship, to the new dose-response model. Two key advantages of the proposed model are that it can capture dose-response relationship from baseline up to target set point, and that it enables linear parameterization, thereby facilitating the control design task. We will ex-

amine the efficacy of the proposed approach using an example of heart rate (HR) response to a vasoactive medication norepinephrine (NE).

4.2 Semi-Adaptive Control Design

Here in this chapter we will use the aforementioned Exponential model in the controller design. For the sake of convenience, we reformulate the Exponential model as follows (Fig 4.1)

$$\dot{I}_e(t) = -k_e I_e(t) + k_e u(t) \triangleq F\big(I_e(t)\big) \tag{4.1a}$$

$$x(t) = 1 - \frac{I_e^{\lambda}(t)}{I_\sigma^{\lambda} + 2I_e^{\lambda}(t)} \tag{4.1b}$$

$$R(t) = R_0\left[1 + k_\sigma \ln \frac{x(t)}{2 - x(t)}\right] \triangleq H\big(I_e(t)\big) \tag{4.1c}$$

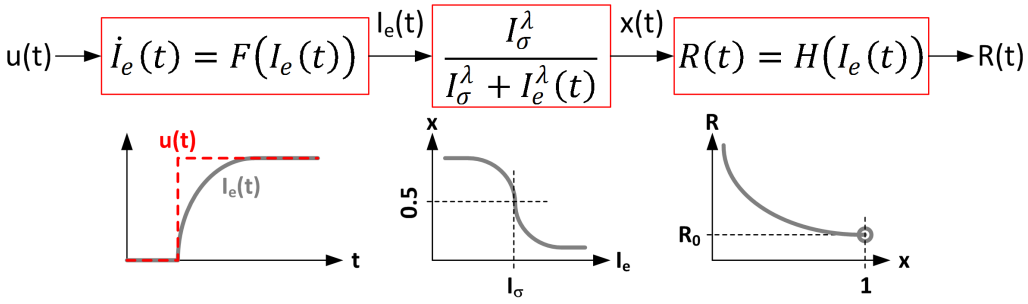

Figure 4.1: Structure of the Exponential model used to describe excitatory dose-response relationships.

where $u(t)$ is the intravenous medication infusion rate, $I_e(t)$ the infusion rate at the (hypothetical) effect site, k_e the time constant associated with the distribution of medication between blood and effect site, $x(t)$ the output of the Emax model with

cooperativity constant λ, $R(t)$ the medication response, R_0 the baseline response (i.e., in the absence of medication infusion), and k_σ a constant specifying the degree of medication effect. This model consists of a classical Emax model eqs. (4.1a) and (4.1b) (in which the minimum response is assumed to be zero, i.e., the maximum dose-dependent effect is equal to R_0; see (4.1b)) and a nonlinear transformation (4.1c) in the form of inverse logistic function. In fact, noting that (4.1c) can be rewritten as follows:

$$x(t) = \frac{2e^{(R(t)-R_0)/(R_0 k\sigma)}}{1 + e^{(R(t)-R_0)/(R_0 k\sigma)}} \tag{4.2}$$

Equation (4.1c) transforms $0 < x(t) \leq 1$ to $R_0 \leq R(t) < \infty$ in case $k < 0$ (Fig. 1). In addition, noting that $x(t) = 1/2$ and $R(t) = R_0[1 - k \ln 3]$ when $I_e(t) = I_\sigma$, I_σ is defined as the effect site infusion rate associated with σ % increase in response $R(t)$ from the baseline R_0 by specifying $k_\sigma = -\sigma / \ln 3$:

$$I_e(t) = I_\sigma \;\rightarrow\; x(t) = \frac{1}{2} \;\rightarrow\; R(t) = R_0[1 - k_\sigma \ln 3] = R_0[1 + \sigma] \tag{4.3}$$

In our prior work, we developed a semi-adaptive control approach to the infusion of medications with depressive dose-response relationship [31]. The key idea of the approach was to enable linear parameterization of the Emax model (eqs. (4.1a) and (4.1b)) by fixing its low-sensitivity parameter λ at a nominal value. To extend the semi-adaptive control paradigm to the Exponential model (4.1), it is of interest to examine the parametric sensitivity associated with this model. As we have shown in Chapter 3.4, λ can be made to be the least sensitivie by setting σ in accordance with the desired target point. Hence, λ can be safely replaced by its population averaged value.

Under the assumption that λ is fixed at a nominal value in (4.1), the Exponential model (4.1) can be cast into a linearly parameterized model. From eqs. (4.1b) and (4.2), $I_e(t)$ can be expressed in terms of $R(t)$ as follows:

$$I_e(t) = I_\sigma \sqrt[\bar{\lambda}]{\frac{1 - e^{(R(t)-R_0)/(k_\sigma R_0)}}{2e^{(R(t)-R_0)/(k_\sigma R_0)}}} \triangleq I_\sigma y(t) \tag{4.4}$$

where $\bar{\lambda}$ is the nominal value of λ. Then, the dynamics associated with $I_e(t)$ in (4.1a) can be expressed in terms of the transformed output variable $y(t)$ as follows:

$$\dot{y}(t) = -k_e y(t) + \frac{k_e}{I_\sigma} u(t) \tag{4.5}$$

which can be linearly parameterized with respect to k_e and k_e/I_σ . Hence, standard adaptive control techniques, such as model reference adaptive control (MRAC) [43], can be employed to regulate $y(t)$, and accordingly, $R(t)$. To this end, consider the following reference model dictating the desired behavior of the closed-loop controlled medication response:

$$\dot{y}_m(t) = -a_m y_m(t) + a_m r(t) \tag{4.6}$$

where $y_m(t)$ is the desired response, $r(t)$ the bounded reference, and a_m a positive constant. The goal of control design is to formulate an adaptive control law to asymptotically drive $y(t)$ towards $y_m(t)$: $\lim_{t\to\infty} y(t) = y_m(t)$. Building upon the MRAC technique, consider the control law given by:

$$u(t) = \widehat{a}_r(t) r(t) + \widehat{a}_y(t) y(t) - p e(t) \tag{4.7}$$

where $e(t) = y(t) - y_m(t)$ is the tracking error, $\hat{a}_r(t)$ and $\hat{a}_y(t)$ the adaptive feedback gains, p the non-adaptive feedback gain. It can be shown that the plant dynamics

(4.5) is perfectly matched to that of the reference model if $\widehat{a}_r(t) = a_r = a_m\frac{I_\sigma}{k_e}$ and $\widehat{a}_y(t) = a_y = (k_e - a_m)\frac{I_\sigma}{k_e}$. Yet, in practice, a_r and a_y are unknown and must be estimated from dose-response data. If we define the discrepancy between a_r and a_y versus $\widehat{a}_r(t)$ and $\widehat{a}_y(t)$ as follows:

$$\widetilde{\boldsymbol{a}}(t) \triangleq \begin{bmatrix} \widetilde{a}_r(t) \\ \\ \widetilde{a}_y(t) \end{bmatrix} = \begin{bmatrix} \widehat{a}_r(t) - a_m\frac{I_\sigma}{k_e} \\ \\ \widehat{a}_y(t) - (k_e - a_m)\frac{I_\sigma}{k_e} \end{bmatrix} \tag{4.8}$$

The dynamics of the tracking error associated with the control law (4.7) is given by:

$$\begin{aligned} \dot{e}(t) &= \dot{y}(t) - \dot{y}_m(t) \\ &= -k_e y + \frac{k_e}{I_\sigma}\big[\widehat{a}_r(t)r(t) + \widehat{a}_y(t)y(t) - pe(t)\big] + a_m y_m(t) - a_m r(t) \\ &= -\left(a_m + \frac{k_e}{I_\sigma}p\right)e(t) + \frac{k_e}{I_\sigma}\big(\widetilde{a}_r(t)r(t) + \widetilde{a}_y(t)y(t)\big) \\ &= -\left(a_m + \frac{k_e}{I_\sigma}p\right)e(t) + \frac{k_e}{I_\sigma}\widetilde{\boldsymbol{a}}^T(t)\boldsymbol{\phi}(t) \end{aligned} \tag{4.9}$$

where $\boldsymbol{\phi}(t) = [r(t), y(t)]^T$. If we emply the following Lyapunov function candidate to design the adaptative law for $\widehat{a}_r(t)$ and $\widehat{a}_y(t)$:

$$V\big(e(t), \widetilde{\boldsymbol{a}}(t)\big) = \frac{1}{2}e^2(t) + \frac{1}{2}\frac{k_e}{I_\sigma}\widetilde{\boldsymbol{a}}^T(t)\boldsymbol{\Gamma}^{-1}\widetilde{\boldsymbol{a}}(t) \tag{4.10}$$

where $\Gamma = \left[\begin{smallmatrix} \gamma_1 & 0 \\ 0 & \gamma_2 \end{smallmatrix}\right]$ and $\gamma_1, \gamma_2 > 0$ are the adaptive gains, the time derivative of the Lyapunov function candidate becomes:

$$\begin{aligned} \dot{V}\big(e(t), \widetilde{\boldsymbol{a}}(t)\big) &= e(t)\dot{e}(t) + \frac{k_e}{I_\sigma}\widetilde{\boldsymbol{a}}^T(t)\boldsymbol{\Gamma}^{-1}\dot{\widetilde{\boldsymbol{a}}}(t) \\ &= e(t)\left[-\left(a_m + \frac{k_e}{I_\sigma}p\right)e(t) + \frac{k_e}{I_\sigma}\widetilde{\boldsymbol{a}}^T(t)\boldsymbol{\phi}(t)\right] + \frac{k_e}{I_\sigma}\widetilde{\boldsymbol{a}}^T(t)\boldsymbol{\Gamma}^{-1}\dot{\widetilde{\boldsymbol{a}}}(t) \end{aligned} \tag{4.11}$$

Hence, $\dot{V}\big(e(t), \widetilde{\boldsymbol{a}}(t)\big)$ can be made negative semi-definite with the following

adaptive law:

$$\dot{\widehat{\boldsymbol{a}}}(t) = \begin{bmatrix} \dot{\widehat{a}}_r(t) \\ \\ \dot{\widehat{a}}_y(t) \end{bmatrix} = -\boldsymbol{\Gamma}\boldsymbol{\phi}(t)e(t) \tag{4.12}$$

Indeed,

$$\dot{V}\big(e(t), \widetilde{\boldsymbol{a}}(t)\big) = -\left(a_m + \frac{k_e}{I_\sigma}p\right)e^2(t) \leq 0 \tag{4.13}$$

Now that $V\big(e(t), \widetilde{\boldsymbol{a}}(t)\big)$ is positive definite and $\dot{V}\big(e(t), \widetilde{\boldsymbol{a}}(t)\big)$ is negative semi-definite, it can be concluded that $V\big(e(t), \widetilde{\boldsymbol{a}}(t)\big)$ is bounded. Hence, the plant (4.5) subject to the control law (4.7) with the adaptive law (4.12) is globally stable, and the signals $e(t)$, $\widetilde{a}_r(t)$, and $\widetilde{a}_y(t)$ are bounded. Then, it can be claimed that $e(t)$ is also bounded from (4.9). This means that $V\big(e(t), \widetilde{\boldsymbol{a}}(t)\big)$ is bounded, and as a consequence, $V\big(e(t), \widetilde{\boldsymbol{a}}(t)\big)$ is uniformly continuous. Therefore, Barbalats Lemma [43] dictates that $\lim_{t\to\infty} V\big(e(t), \widetilde{\boldsymbol{a}}(t)\big) = 0$, which, together with (4.13), leads to $\lim_{t\to\infty} e(t) = 0$.

4.3 Semi-Adaptive Control Evaluation

To validate and analyze the efficacy of the semi-adaptive control based on the proposed new dose-response model, we conducted a set of in-silico testing as follows. First, we constructed 100 in-silico subjects as plant models in the form of the Emax model (3.22), by randomizing its parameters within the respective parametric range obtained from the Emax models identified for all the animals while setting $\bar{R}_0 = 118$. Second, we simulated the proposed semi-adaptive control law (4.7) and (4.12) in these plant models. Especially, we simulated the control law with r(t) corresponding to the set points of 25 %, 50 %, and 75 % increase in HR response with respect to the baseline (hence a total of 300 in-silico tests) to examine the

efficacy of the controller across diverse target set points. For each given set point, we incorporated the corresponding value of σ in control design, i.e., in transforming $R(t)$ to $y(t)$ via (4.4). We likewise simulated a non-adaptive controller (in which $\dot{\widehat{a}}_r(t) = \dot{\widehat{a}}_y(t) = 0$ in (4.12) with $\widehat{a}_r(t) = a_m \frac{\bar{I}_\sigma}{\bar{k}_e}$ and $\widehat{a}_y(t) = (\bar{k}_e - a_m)\frac{\bar{I}_\sigma}{\bar{k}_e}\, \forall t$, where $\bar{k}_e$ and $\bar{I}_\sigma$ are nominal values) under the same scenarios to compare semi-adaptive and non-adaptive controls. Third, we quantified the performance of the controllers in terms of the speed of response (5 % settling time), root-mean-squared error (RMSE) during the transient (defined as the first 9.5 min of HR response), and steady-state error. Fourth, we examined the quality of the parameters estimated by the adaptive law (4.12) by computing the discrepancy between true versus estimated I_σ in the steady state in all the subjects associated with all the set points.

To perform realistic in-silico testing, we incorporate the following details. First, we simulate measurement noise: we use a zero-mean white noise with a standard deviation (SD) of 1.4 bpm based on the noise characteristics observed from our experimental data. Second, we simulate zero-order-hold and quantization to account for finite temporal and spatial resolutions in controller computation: we use 1 Hz sensing and control update rates as well as 1 bpm HR resolution. Third, we robustify the control law: we augment the control law with (i) a 15-th order causal moving average filter to mitigate the adverse influence of measurement noise; and (ii) a dead zone scheme to prevent the drift of parameter estimates when the patients HR response is regulated at a target set point.

To produce 100 randomized Emax models, we use the following parametric envelopes obtained from system identification: $0.11\text{min}^{-1} \leq k_e \leq 0.94\,\text{min}^{-1}$,

$0.20\,\text{mcg/kg/min} \leq I_{50} \leq 0.43\,\text{mcg/kg/min}$, and $1.1 \leq \lambda \leq 3.6$. To implement the semi-adaptive control law, we use the following parameters: $a_m = 0.3\,\text{min}^{-1}$, $\Gamma = \left[\begin{smallmatrix} -3 & 0 \\ 0 & -5 \end{smallmatrix}\right]$, and $p = 2.5$. In addition, we set a dead zone width of 2.0 bpm considering the measurement noise characteristics.

4.3.1 Results and Discussion

Table. 4.1 summarizes the performance of semi-adaptive control relative to non-adaptive control in terms of transient and steady-state characteristics, while Fig. 4.3 illustrates representative in-silico testing cases associated with semi-adaptive versus non-adaptive control. Here, we selected the best and worst cases as follows: (i) we normalized the transient RMSE and steady-state error in each individual by their respective mean values; (ii) we computed the aggregated error associated with each individual as the sum of the normalized transient RMSE and steady-state error; and (iii) we selected the best and worst cases as the individuals associated with minimum and maximum aggregated error, respectively. Overall, semi-adaptive control achieved superior consistency in transient response to its non-adaptive counterpart: (i) its 5% settling time was persistently close to the target value of 10.0 min while non-adaptive control suffered from large variability (up to 76% from the target in terms of mean value); and (ii) RMSE in reference model tracking during the transient was $> 30\%$ smaller in semi-adaptive than in non-adaptive control. In addition, semi-adaptive control outperformed non-adaptive control in terms of steady-state performance as well: the mean and standard deviation of absolute HR

error in the steady state were $> 41.3\%$ and $> 17\%$ smaller in semi-adaptive than in non-adaptive control, despite the dead zone scheme incorporated in the former that negatively impacted its steady-state tracking performance. The standard deviation of transient RMSE (both SA and NA cases) and steady-state error (NA) is rougly proportional to the amount of increase of HR (see Fig. 4.2), which is as expected due to the random distribution of the parameters of the random subjects. The standard deviation of steady-state error in SA case is almost constant despite of the σ value because it is only affected by dead-zone and white noise (since I_σ estimate will converge to its true value in the end) and thus it is much smaller than that of NA case. In sum, the results strongly indicate that semi-adaptive control is superior to its non-adaptive counterpart in achieving uniform response characteristics against large inter-individual variability in dose-response relationship.

Set Point (% HR Change)	Control	Settling Time [min] (Target: 10.0 min)	Transient RMSE [bpm]	Steady-state Error [bpm]
25	SA	9.35 ± 1.33	1.05 ± 0.128	0.810 ± 0.528
	NA	8.51 ± 1.64	1.50 ± 0.220	1.38 ± 0.636
50	SA	10.5 ± 0.766	1.12 ± 0.213	0.601 ± 0.403
	NA	13.0 ± 1.79	2.14 ± 0.582	2.20 ± 0.690
75	SA	10.7 ± 0.566	1.40 ± 0.281	0.745 ± 0.533
	NA	17.6 ± 2.24	4.96 ± 1.59	5.82 ± 1.79

Table 4.1: Performance of semi-adaptive and non-adaptive controllers associated with 25%, 50%, and 75% change in set point response with respect to the baseline. SA: semi-adaptive control. NA: non-adaptive control.

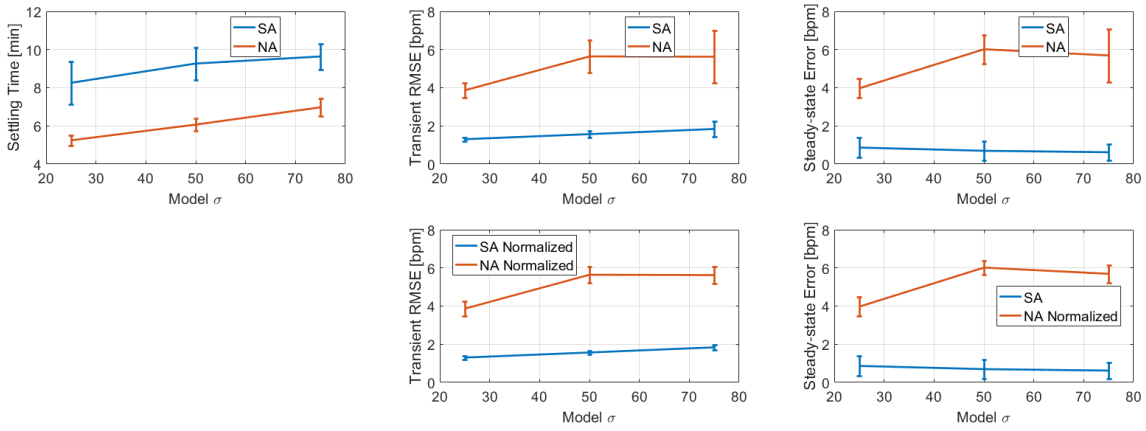

Figure 4.2: Errorbar plot of the controller performance comparison in Table. 4.1.

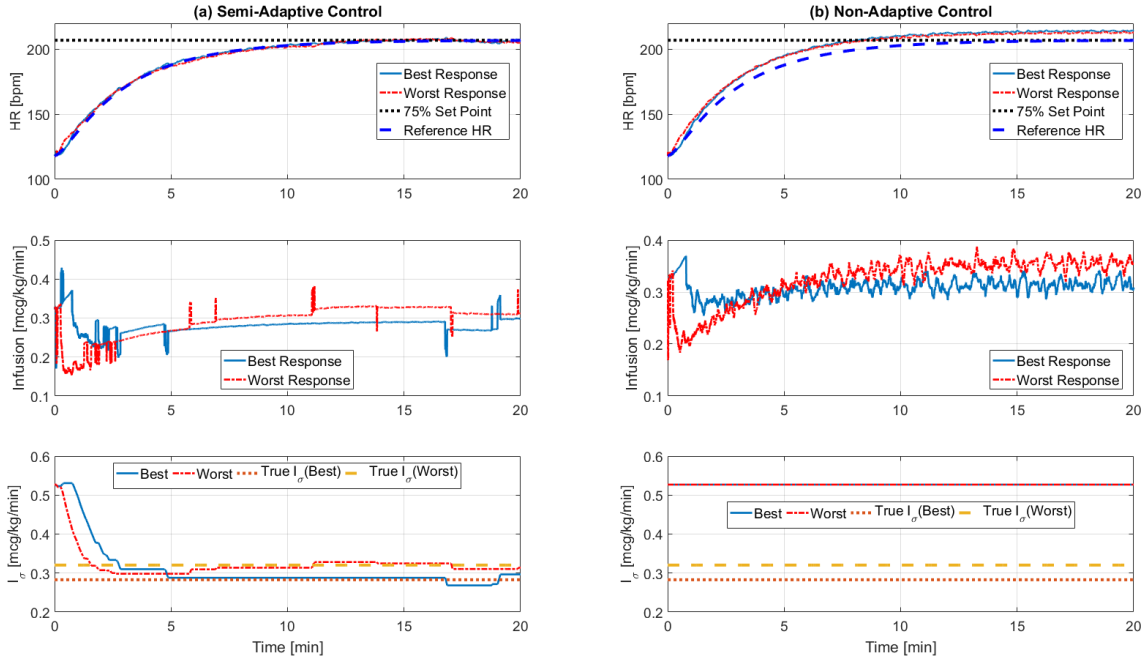

Figure 4.3: Representative in-silico testing cases. (a) Semi-adaptive control. (b) Non-adaptive control.

Note that, although the influence of λ on the steady-state performance of semi-adaptive control can be removed by setting σ according to the target set point, its influence on transient response may still persist. In particular, λ smaller (greater) than its nominal value tends to elicit fast (slow) transient response through an increase in the dose-response sensitivity, and I_σ smaller (greater) than its nominal value, as well as k_e greater (smaller) than its nominal value, exert an synergistic influence on this tendency through a further increase in the dose-response sensitivity and the speed of medication distribution dynamics.

Fig. 4.4 presents the distribution of I_σ errors associated with the semi-adaptive control in response to 25%, 50%, and 75% target set points (N=100 each). The estimates of I_σ were highly accurate regardless of target set point ($< 8.6\%$), which may not be surprising considering the large sensitivity of the systems response to I_σ (Fig. 3.15). But more obviously, it is expected to be estimated without any error in theory, because I_σ is nothing but the infusion rate in the steady state when σ is set to the % change in response from the baseline. In fact, the small errors shown in Fig. 4.4 were incurred mostly due to the dead zone scheme, which stopped adaptation under small set point tracking errors, as well as the measurement noise. The ability to accurately estimate I_σ is an advantage in that the knowledge of I_σ may be useful in securing the safety of semi-adaptive control by preventing the infusion of unacceptably high dose beyond the therapeutic limit of each patient.

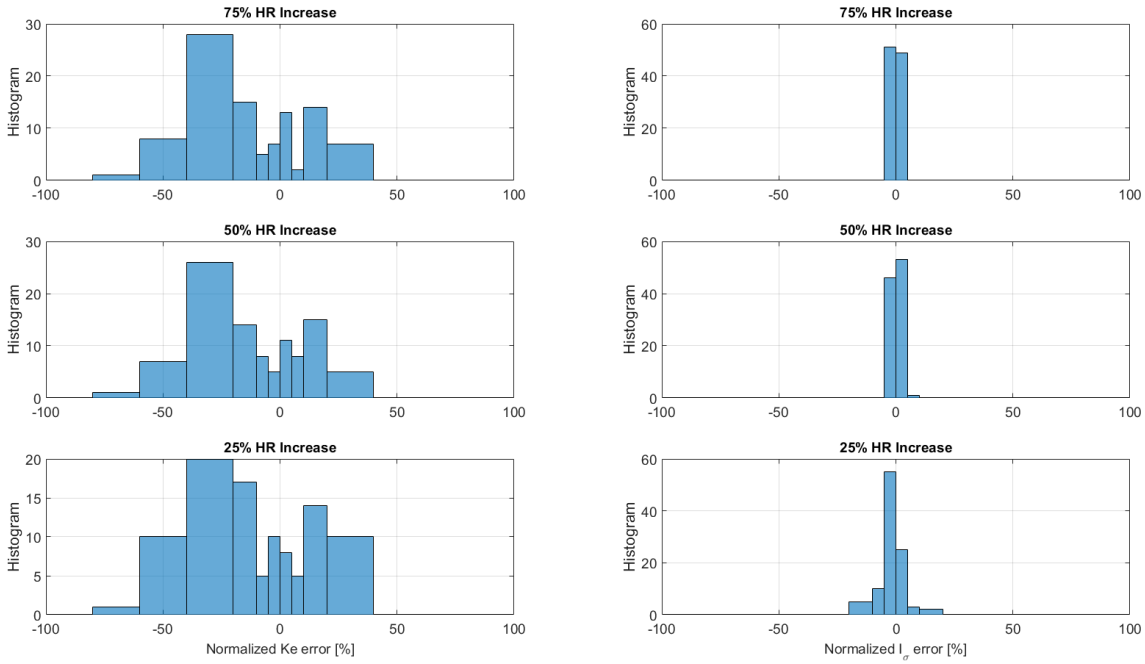

Figure 4.4: Distribution of I_σ errors associated with semi-adaptive control in response to 25%, 50%, and 75% target set points.

Chapter 5: Conclusions and Future Works

In this thesis we have proposed a new dose-response model to describe excitatory dose-dependent effects and presented the application of a semi-adaptive control approach to this model using norepinephrine (NE) as the drug and heart rate (HR) as the desired endpoint. An immediate extension to this work would be to consider a multi-input-multi-output version of the system, i.e., infusion of multiple vasopressors and simultaneous control of multiple endpoints. Besides, the proposed semi-adaptive controller along with the new model has not been used and tested in any in-vivo animal experiments, and thus it remains a question as to how good the controller would perform in the real experiments despite of the good results obtained from in-silico computer simulations. Since in the simulation we used Emax model to generate the hypothetical HR response and the response from a real animal would undoubtedly be different from that, therefore an in-vivo experiment is needed to evaluate the efficacy of the proposed controller.

Besides, the DDDR model used in this new model assumes no time-delay, i.e., the drug arrives at the effect site immediately after the infusion. Although there is no obvious evidence from the experimental data supporting the existence of the time-delay in the system, it is still counter-intuitive to believe that the drug

achieves instantaneous distribution at the effect site. Hence, it might be interesting to introduce time-delay into the system. By doing so, the stability of the controller also needs to be reconsidered since time-delay in the feedback process can seriously deteriorate the performance of the controller.

Additionally, it might also be of interest to investigate the accurateness of Emax model as the base model. It is shown in the area of anesthesia control that the parameters of Emax model (EC_{50} and shape factor λ) are different for induction and recovery [44], i.e., loss of consciousness and recovery of consciousness might be two asymmetrical processes. Although there has not been reports with similar evidence on the vasopressor, it is definitely worth the time and effort to better understand the underlying mechanism of vasopressors, ideally all the way down to the molecular level so that models that better describe the process could be invented.

In the controller simulation, the artificial pump delivers whatever infusion rate that is obtained by the adaptive law. In many of the cases, spikes, i.e., the abrupt change in the infusion rate, appears during the infusion. In reality, however, the actual infusion profile would be much smoother than its theoretical counterpart because the pump itself is subject to its own dynamics. It takes time for the pump to start or stop the infusion or to transit to a new infusion rate, but the pump dynamics is not considered in the simulation. Therefore, future work may consider incorporating the pump dynamics (perhaps as a first-order system) to the entire model so that the calculated infusion rate can be more realistic.

Besides, it is assumed that baseline value of HR can be accurately obtained in this work, which is normally the case because it can be obtained by making

the patient lie down on the bed doing nothing and then average the measured HR during the period. However, for those who suffer from severe injuries and are sent to the hospital for emergent treatment, it is neither ethical to waste precious time to try to measure the baseline value of various endpoints, nor it is possible to do this because the endpoints of these patients are already far away from normal values and are changing rapidly due to the injuries. Thus, the effect of not being able to have accurate baseline value should also be studied.

Ultimately, since closed-loop control of infusion control is only a part of the bigger picture, which is to develop a fully automated critical care monitoring system, it is of great importance to understand how to put different subsystems together and have them work seamlessly without any conflicts.

Bibliography

[1] D. Annane, P. Aegerter, M. Jars-Guincestre, and B. Guidet, "Current epidemiology of septic shock: the cub-rea network," *Am J Respir Crit Care Med*, vol. 168, no. 2, pp. 165–72, July 2003.

[2] D. Angus, W. Linde-Zwirble, J. Lidicker, G. Clermont, J. Carcillo, and M. Pinsky, "Epidemiology of severe sepsis in the united states: analysis of incidence, outcome, and associated costs of care," *Critical care medicine*, vol. 29, no. 7, pp. 1303–1310, 2001.

[3] R. J. Beale, S. M. Hollenberg, J.-L. Vincent, and J. E. Parrillo, "Vasopressor and inotropic support in septic shock: an evidence-based review," *Critical care medicine*, vol. 32, no. 11, pp. S455–S465, 2004.

[4] R. Bone, R. Balk, F. Cerra, R. Dellinger, A. Fein, W. Knaus, R. Schein, and W. Sibbald, "Definitions for sepsis and organ failure and guidelines for the use of innovative therapies in sepsis," *Chest*, vol. 101, no. 6, pp. 1644–55, Jun 1992.

[5] Dellinger RP, Levy MM, Carlet JM, et al; International Surviving Sepsis Campaign Guidelines Committee; American Association of Critical-Care Nurses; American College of Chest Physicians; American College of Emergency Physicians; Canadian Critical Care Society; European Society of Clinical Microbiology and Infectious Diseases; European Society of Intensive Care Medicine; European Respiratory Society; International Sepsis Forum; Japanese Association for Acute Medicine; Japanese Society of Intensive Care Medicine; Society of Critical Care Medicine; Society of Hospital Medicine; Surgical Infection Society; World Federation of Societies of Intensive and Critical Care Medicine, "Surviving sepsis campaign: international guidelines for management of severe sepsis and septic shock: 2008," *Crit Care Med*, vol. 36, no. 1, pp. 296–327, 2008.

[6] C. B. Overgaard and V. Džavík, "Inotropes and vasopressors," *Circulation*, vol. 118, no. 10, pp. 1047–1056, 2008.

[7] H. Derendorf and B. Meibohm, "Modeling of pharmacokinetic/pharmacodynamic (pk/pd) relationships: concepts and perspectives," *Pharmaceutical research*, vol. 16, no. 2, pp. 176–85, 1999.

[8] J. Schuttler and H. Ihmsen, "Population pharmacokinetics of propofola multicenter study," *The Journal of the American Society of Anesthesiologists*, vol. 92, no. 3, pp. 727–738, 2000.

[9] G. A. Dumont and J. M. Ansermino, "Closed-loop control of anesthesia: a primer for anesthesiologists," *Anesthesia & Analgesia*, vol. 117, no. 5, pp. 1130–1138, 2013.

[10] W. M. Haddad, J. M. Bailey, B. Gholami, and A. R. Tannenbaum, "Clinical decision support and closed-loop control for intensive care unit sedation," *Asian Journal of Control*, vol. 15, no. 2, pp. 317–339, 2013. [Online]. Available: http://dx.doi.org/10.1002/asjc.701

[11] A. R. Absalom, R. De Keyser, and M. M. Struys, "Closed loop anesthesia: are we getting close to finding the holy grail?" *Anesthesia & Analgesia*, vol. 112, no. 3, pp. 516–518, 2011.

[12] M. M. Struys, E. P. Mortier, and T. D. Smet, "Closed loops in anaesthesia," *Best Practice & Research Clinical Anaesthesiology*, vol. 20, no. 1, pp. 211–220, 2006, monitoring Consciousness. [Online]. Available: http://www.sciencedirect.com/science/article/pii/S1521689605000698

[13] G. E. Van Poucke, L. J. Bravo, and S. L. Shafer, "Target controlled infusions: targeting the effect site while limiting peak plasma concentration," *IEEE transactions on biomedical engineering*, vol. 51, no. 11, pp. 1869–1875, 2004.

[14] J. Glen, "The development of diprifusor: a tci system for propofol," *Anaesthesia*, vol. 53, no. s1, pp. 13–21, 1998.

[15] N. Liu, T. Chazot, A. Genty, A. Landais, A. Restoux, K. McGee, P.-A. Laloë, B. Trillat, L. Barvais, and M. Fischler, "Titration of propofol for anesthetic induction and maintenance guided by the bispectral index: Closed-loop versus manual controla prospective, randomized, multicenter study," *The Journal of the American Society of Anesthesiologists*, vol. 104, no. 4, pp. 686–695, 2006.

[16] T. De Smet, M. M. Struys, M. M. Neckebroek, K. Van den Hauwe, S. Bonte, and E. P. Mortier, "The accuracy and clinical feasibility of a new bayesian-based closed-loop control system for propofol administration using the bispectral index as a controlled variable," *Anesthesia & Analgesia*, vol. 107, no. 4, pp. 1200–1210, 2008.

[17] T. M. Hemmerling, S. Charabati, C. Zaouter, C. Minardi, and P. A. Mathieu, "A randomized controlled trial demonstrates that a novel closed-loop propofol system performs better hypnosis control than manual administration," *Can J Anaesth*, vol. 57, no. 8, pp. 725–35, 2010.

[18] W. M. Haddad, T. Hayakawa, and J. M. Bailey, "Adaptive control for nonnegative and compartmental dynamical systems with applications to general anesthesia," *International Journal of Adaptive Control and Signal Processing*, vol. 17, no. 3, pp. 209–235, 2003.

[19] J.-O. Hahn, G. A. Dumont, and J. M. Ansermino, "Robust closed-loop control of hypnosis with propofol using wav cns index as the controlled variable," *Biomedical Signal Processing and Control*, vol. 7, no. 5, pp. 517–524, 2012.

[20] J. Macdougall, *Analysis of Dose–Response Studies—Emax Model*. New York, NY: Springer New York, 2006, pp. 127–145. [Online]. Available: http://dx.doi.org/10.1007/0-387-33706-7_9

[21] K. Soltesz, J.-O. Hahn, T. Hägglund, G. A. Dumont, and J. M. Ansermino, "Individualized closed-loop control of propofol anesthesia: a preliminary study," *Biomedical Signal Processing and Control*, vol. 8, no. 6, pp. 500–508, 2013.

[22] N. West, G. A. Dumont, K. Heusden, C. L. Petersen, S. Khosravi, K. Soltesz, A. Umedaly, E. Reimer, and J. M. Ansermino, "Robust closed-loop control of induction and maintenance of propofol anesthesia in children," *Pediatric Anesthesia*, vol. 23, no. 8, pp. 712–719, 2013.

[23] G. A. Dumont, A. Martinez, and J. M. Ansermino, "Robust control of depth of anesthesia," *International Journal of Adaptive Control and Signal Processing*, vol. 23, no. 5, pp. 435–454, 2009. [Online]. Available: http://dx.doi.org/10.1002/acs.1087

[24] C. M. Ionescu, R. D. Keyser, B. C. Torrico, T. D. Smet, M. M. Struys, and J. E. Normey-Rico, "Robust predictive control strategy applied for propofol dosing using bis as a controlled variable during anesthesia," *IEEE Transactions on Biomedical Engineering*, vol. 55, no. 9, pp. 2161–2170, Sept 2008.

[25] A. Gentilini, C. W. Frei, A. H. Glattfedler, M. Morari, T. J. Sieber, R. Wymann, T. W. Schnider, and A. M. Zbinden, "Multitasked closed-loop control in anesthesia," *IEEE Engineering in Medicine and Biology Magazine*, vol. 20, no. 1, pp. 39–53, Jan 2001.

[26] T. De Smet, M. M. Struys, S. Greenwald, E. P. Mortier, and S. L. Shafer, "Estimation of optimal modeling weights for a bayesian-based closed-loop system for propofol administration using the bispectral index as a controlled variable: a simulation study," *Anesthesia & Analgesia*, vol. 105, no. 6, pp. 1629–1638, 2007.

[27] C. M. Ionescu, R. Hodrea, and R. D. Keyser, "Variable time-delay estimation for anesthesia control during intensive care," *IEEE Transactions on Biomedical Engineering*, vol. 58, no. 2, pp. 363–369, Feb 2011.

[28] J. Nio, R. De Keyser, S. Syafiie, C. Ionescu, and M. Struys, "Epsac-controlled anesthesia with online gain adaptation," *International Journal of Adaptive Control and Signal Processing*, vol. 23, no. 5, pp. 455–471, 2009. [Online]. Available: http://dx.doi.org/10.1002/acs.1073

[29] S. Dhillon, *Clinical Pharmacokinetics*. Pharmaceutical Press, 2006.

[30] J. O. Hahn, G. A. Dumont, and J. M. Ansermino, "A direct dynamic dose-response model of propofol for individualized anesthesia care," *IEEE Trans. Biomed. Eng*, no. 59, pp. 571–578, 2012.

[31] X. Jin, C.-S. Kim, G. A. Dumont, J. M. Ansermino, and J.-O. Hahn, "A semi-adaptive control approach to closed-loop medication infusion," *International Journal of Adaptive Control and Signal Processing*, vol. 31, no. 2, pp. 240–254, 2017. [Online]. Available: http://dx.doi.org/10.1002/acs.2696

[32] Y. Hashimoto and L. B. Sheiner, "Designs for population pharmacodynamics: Value of pharmacokinetic data and population analysis," *J. Pharmacokinet. Biopharm*, vol. 19, pp. 333–53, 1991.

[33] G. A. Dumont, "Closed-loop control of anesthesia - a review," *IFAC Proceedings Volumes*, vol. 45, no. 18, pp. 373–378, 2012. [Online]. Available: http://www.sciencedirect.com/science/article/pii/S1474667016321279

[34] The Mathworks, Inc. (2017) Documentation on optimization toolbox. [Online]. Available: https://www.mathworks.com/help/pdf_doc/optim/optim_tb.pdf

[35] M. Anguelova, "Observability and identifiability of nonlinear systems with applications in biology," Ph.D. dissertation, Chalmers University of Technology, Gothenburg, Sweden, 2007. [Online]. Available: http://www.math.chalmers.se/Math/Research/Preprints/Doctoral/2007/3.pdf

[36] H. K. Khalil, *Nonlinear Systems*, 3rd ed. New Jersey: Pearson, 12 2001.

[37] H. Singh, "Bispectral index (bis) monitoring during propofol-induced sedation and anaesthesia," *European journal of anaesthesiology*, vol. 16, no. 01, pp. 31–36, 1999.

[38] M. Kisilewicz, H. Rosenberg, and C. Vaillancourt, "Remifentanil for procedural sedation: a systematic review of the literature," *Emergency Medicine Journal*, 2017. [Online]. Available: http://emj.bmj.com/content/early/2017/02/28/emermed-2016-206129

[39] J. M. Ansermino, P. Brooks, D. Rosen, C. A Vandebeek, and C. Reichert, "Spontaneous ventilation with remifentanil in children," *Pediatric Anesthesia*, vol. 15, no. 2, pp. 115–121, 2005.

[40] K. Uemura, A. Kamiya, I. Hidaka, T. Kawada, S. Shimizu, T. Shishido, M. Yoshizawa, M. Sugimachi, and K. Sunagawa, "Automated drug delivery system to control systemic arterial pressure, cardiac output, and left heart filling pressure in acute decompensated heart failure," *Journal of applied physiology*, vol. 100, no. 4, pp. 1278–1286, 2006.

[41] B. L. Sng, H. S. Tan, and A. T. H. Sia, "Closed-loop double-vasopressor automated system vs manual bolus vasopressor to treat hypotension during spinal anaesthesia for caesarean section: a randomised controlled trial," *Anaesthesia*, vol. 69, no. 1, pp. 37–45, 2014. [Online]. Available: http://dx.doi.org/10.1111/anae.12460

[42] M. Merouani, B. Guignard, F. Vincent, S. W. Borron, P. Karoubi, J.-P. Fosse, Y. Cohen, C. Clec'h, E. Vicaut, C. Marbeuf-Gueye, F. Lapostolle, and F. Adnet, "Norepinephrine weaning in septic shock patients by closed loop control based on fuzzy logic," *Critical Care*, vol. 12, no. 6, p. R155, 2008. [Online]. Available: http://dx.doi.org/10.1186/cc7149

[43] J.-J. E. Slotine and W. Li, *Applied nonlinear control*. Englewood Cliffs, NJ: Prentice-Hall, 1991.

[44] I. D. McKay, L. J. Voss, J. W. Sleigh, J. P. Barnard, and E. K. Johannsen, "Pharmacokinetic-pharmacodynamic modeling the hypnotic effect of sevoflurane using the spectral entropy of the electroencephalogram," *Anesthesia & Analgesia*, vol. 102, no. 1, pp. 91–97, 2006.